

1 **A HTAP multi-model assessment of the influence of regional**
2 **anthropogenic emission reductions on aerosol direct radiative forcing**
3 **and the role of intercontinental transport**

4
5 Hongbin Yu^{1,2}, Mian Chin², J. Jason West³, Cynthia S. Atherton⁴, Nicolas Bellouin⁵,
6 Dan Bergmann⁴, Isabelle Bey⁶, Huisheng Bian^{7,2}, Thomas Diehl^{8,2}, Gerd Forberth⁵,
7 Peter Hess⁹, Michael Schulz¹⁰, Drew Shindell¹¹, Toshihiko Takemura¹², Qian Tan^{8,2}

- 8
9 1. Earth System Science Interdisciplinary Center, University of Maryland,
10 College Park, Maryland, 20740, USA
11 2. Earth Science Directorate, NASA Goddard Space Flight Center, Greenbelt,
12 Maryland, 20771, USA
13 3. Department of Environmental Sciences and Engineering, University of North
14 Carolina, Chapel Hill, NC 27599, USA
15 4. Atmospheric Earth and Energy Division, Lawrence Livermore National
16 Laboratory, Livermore CA 94551, USA
17 5. Met Office Hadley Centre, FitzRoy Road, Exeter Devon, EX1 3PB, UK
18 6. Center for Climate Systems Modeling, ETH Zurich, Universitatstrasse 16, 8092
19 Zurich, Switzerland
20 7. Joint Center for Earth Systems Technology, University of Maryland at Baltimore
21 County, Baltimore, Maryland, 21228, USA
22 8. Universities Space Research Association, Columbia, Maryland, 21044, USA
23 9. Biological and Environmental Engineering, Cornell University, Ithaca, New
24 York, 14850, USA
25 10. Meteorologisk Institutt, Postboks 43 Blindern 0313, Oslo, Norway
26 11. NASA Goddard Institute for Space Studies, New York, New York, 10025, USA
27 12. Research Institute for Applied Mechanics, Kyushu University, Japan

28
29
30 **Correspondence**

31
32 Hongbin Yu
33 NASA GSFC Code 613
34 Greenbelt, MD 20771, USA
35 Hongbin.Yu@nasa.gov
36 301-614-6209
37

38 **Abstract** In this study, we assess changes of aerosol optical depth (AOD) and direct
39 radiative forcing (DRF) in response to the reduction of anthropogenic emissions in four
40 major pollution regions in the northern hemisphere by using results from 10 global
41 chemical transport models in the framework of the Hemispheric Transport of Air
42 Pollution (HTAP). The multi-model results show that on average, a 20% reduction of
43 anthropogenic emissions in North America, Europe, East Asia and South Asia lowers the
44 global mean AOD and DRF by about 9%, 4%, and 10% for sulfate, organic matter, and
45 black carbon aerosol, respectively. The impacts of the regional emission reductions on
46 AOD and DRF extend well beyond the source regions because of intercontinental
47 transport. On an annual basis, intercontinental transport accounts for 10-30% of the
48 overall AOD and DRF in a receptor region, with domestic emissions accounting for the
49 remainder, depending on regions and species. While South Asia is most influenced by
50 import of sulfate aerosol from Europe, North America is most influenced by import of
51 black carbon from East Asia. Results show a large spread among models, highlighting the
52 need to improve aerosol processes in models and evaluate and constrain models with
53 observations.
54

55 **1. Introduction**

56 Anthropogenic aerosols make significant contributions to the global mean radiative
57 forcing (RF) of climate [Forster et al., 2007] by scattering and absorbing solar radiation
58 (so-called “aerosol direct effects”) [McCormick and Ludwig, 1967] and modifying cloud
59 properties, amount, and evolution (collectively referred to as “aerosol indirect effects”)
60 [Twomey, 1977; Gunn and Phillips, 1957; Albrecht, 1989]. RF is a measure of the
61 change of net radiation (incoming minus outgoing) at the top of atmosphere (TOA), at the
62 surface, or within the atmosphere, due to perturbations in atmospheric compositions or
63 surface properties. On a global average basis, the sum of direct and indirect RF at TOA
64 by anthropogenic aerosol is estimated to be -1.2 W m^{-2} [-2.4 to -0.6 W m^{-2}] (cooling)
65 over the period of 1750-2000, which is significant compared to the positive (warming)
66 forcing of $+2.63 [\pm 0.26] \text{ W m}^{-2}$ by anthropogenic long-lived greenhouse gases over the
67 same period [Forster et al., 2007]. In heavily polluted regions, aerosol cooling
68 overwhelms greenhouse warming [Ramanathan et al., 2001; Li et al., 2010]. At the
69 surface, aerosol RF can be much stronger than that at TOA because of aerosol absorption
70 [Satheesh and Ramanathan, 2000]. Currently, uncertainties associated with aerosol RF
71 make the largest contribution to the overall uncertainty in anthropogenic radiative forcing
72 of climate [Forster et al., 2007]. Because of the significant role of aerosols in modulating
73 the Earth’s radiative budget, it is necessary from both scientific and policy perspective to
74 assess how emission changes associated with economic development and
75 regional/national regulations will influence the aerosol radiative forcing.

76

77 The response of global aerosol RF to a fractional change of anthropogenic emissions
78 would depend on the source locations, magnitude, and composition of emitted aerosols
79 and aerosol precursors. While scattering aerosols like sulfate cause a cooling effect,
80 strongly absorbing black carbon aerosols cause warming. Aerosol RF is also determined
81 by several environmental factors such as surface albedo and meteorological conditions
82 (in particular the amount and distribution of clouds and winds). With these differences,
83 the aerosol RF per unit change of regional emissions would differ from one region to
84 another. It is also important to note that the impact of a regional emission reduction is not
85 confined to the region itself. Instead regional emission reductions can have far reaching
86 impacts on RF in downwind regions, because of intercontinental transport of
87 anthropogenic aerosols. Long-range transport has been observed by long-term surface
88 monitoring networks [*Prospero et al., 2003; VanCuren, 2003; Fischer et al., 2010*], in-
89 situ measurements from intensive field campaigns [*Ramanathan et al., 2007; Clarke and*
90 *Kapustin, 2010*], and satellite observations [*Yu et al., 2008; Rudich et al., 2008; Dirksen*
91 *et al., 2009*] backed by model simulations [*Heald et al., 2006; Chin et al., 2007; Hadley*
92 *et al., 2007*]. Thus how a region is influenced by extraregional emissions is of particular
93 importance for formulating an effective strategy for mitigating regional climate change
94 and combating air pollution. The United Nations Economic Commission for Europe has
95 established a Task Force on Hemispheric Transport of Air Pollutants (HTAP) to
96 understand the growing body of scientific evidence of intercontinental transport and
97 assess its impacts on air quality, climate, and ecosystems [*HTAP, 2010*].
98

99 Modeling studies can offer valuable insights into the relative significance of aerosols
100 from different regions in influencing climate and important implications for formulating
101 effective emission control strategies. Several recent studies have assessed how aerosols
102 emitted in a region or from specific sectors could affect climate in downwind regions
103 [e.g., Reddy and Boucher, 2007; Koch et al., 2007; Shindell et al., 2008a, 2008b]. Other
104 studies have shown that large intermodel differences exist in aerosol lifetime cycle and
105 radiative effect [Kinne et al., 2006; Schulz et al., 2006; Textor et al., 2006], which might
106 undermine the robustness of the results from single model or very limited number of
107 models. Complementary to the prior studies, we use in this study an ensemble of 10
108 global chemical transport or general circulation models to assess the change of global and
109 regional aerosol optical depth (AOD) and direct radiative forcing (DRF) in response to
110 20% reductions of emissions from four major polluted regions in the Northern
111 Hemisphere. These models conducted aerosol source-receptor (S/R) relationship
112 experiments in the HTAP coordinated studies (HTAP 2010). These multi-model S/R
113 experiments allow us to examine a probable range of contributions of intercontinental
114 transport (ICT) relative to intra-regional emissions in determining regional AOD and
115 DRF and help characterize the robustness of the results. Fry et al. [2012] conduct similar
116 analysis of ozone radiative forcing due to 20% reductions of ozone precursor emissions
117 using results from multiple HTAP models.

118

119 The rest of this paper is organized as follows. Section 2 describes the S/R model
120 simulations and analysis methodology, including AOD from the HTAP anthropogenic
121 S/R experiment used in this study and an estimate of the aerosol DRF. Section 3 presents

122 a multi-model analysis of the impacts of 20% reductions of regional anthropogenic
123 emissions on global and regional AOD and DRF and the role of ICT relative to intra-
124 regional emissions. This assessment does not address aerosol indirect effects, or warming
125 effects resulting from BC deposition on snow and ice. We also neglect interactions of
126 aerosols with thermal infrared radiation, as anthropogenic aerosols have relatively small
127 size and their interactions with infrared radiation are minor. Finally, we neglect the
128 radiative forcing of gas-phase components that may have been influenced by these
129 emissions, which were modeled by Fry et al. (2012). Major conclusions from the analysis
130 are summarized and discussed in Section 4.

131

132 **2. Description of model simulations and analysis methodology**

133 **2.1. HTAP modeling experiments on S/R relationships**

134 We use the results from an ensemble of 10 global chemical transport or general
135 circulation models, listed in **Table 1**, to evaluate changes in AOD and DRF in response
136 to a 20% reduction of anthropogenic emissions in four major pollution regions in the
137 Northern Hemisphere under the framework of the HTAP S/R modeling experiments
138 [*Fiore et al., 2009; HTAP, 2010*]. The S/R experiments include a baseline simulation and
139 four perturbation simulations, for which each model submitted monthly AOD fields. For
140 each model, the baseline simulation (SR1) is conducted using emissions and meteorology
141 for 2001. Note that individual models use their own preferred anthropogenic and natural
142 emissions. Each of the four perturbation runs (SR6) represents a 20% reduction in
143 anthropogenic emissions (including biomass burning and n=both gas-phase and aerosol
144 components) in one of four major pollution regions in Northern Hemisphere, namely

145 North America (NA), Europe (EU), East Asia (EA), and South Asia (SA), as illustrated in
146 **Figure 1**. These perturbation model experiments are denoted as SR6NA, SR6EU,
147 SR6EA, and SR6SA, respectively. Also shown in Figure 1 are regional and annual
148 anthropogenic emissions of sulfur dioxide (SO₂), primary particulate organic matter
149 (POM), and black carbon (BC) from 8 models (emissions for ECHAM5 and HadGEM2
150 were not archived and can not be retrieved for this analysis). Clearly anthropogenic
151 emissions show large regional differences. For example, South Asia has the least SO₂
152 emissions that are a factor of 2-4 smaller than the other regions. East Asia has the largest
153 BC emissions that are nearly double the emissions in Europe or South Asia and more
154 than triple the emissions in North America. The regional differences in emissions in
155 combination with the proximity of regions (e.g., the SA region is adjacent to and
156 downwind of the EU region), ICT pathways, and removal/production mechanisms during
157 the transport, would determine the relative roles of ICT and regional emissions, as we
158 will discuss later in the paper.

159

160 **2.2 AOD from HTAP S/R experiments**

161 The major HTAP model outputs used in this study are monthly average AOD (τ) at 550
162 nm for sulfate (SO₄), POM, and BC from individual models. **Figure 2** shows annual
163 average AOD in ambient conditions for a combination of SO₄, POM, and BC from 9
164 models. ECHAM5 simulations are not shown here because the model calculates AOD for
165 dry sulfate, POM, and BC. Although the model also provides water optical depth
166 associated with total aerosol (e.g., due to aerosol humidification), it is impossible,
167 without further uncertain assumptions, to partition the water optical depth into that

168 associated with individual aerosol components. Note that these AOD outputs include both
169 anthropogenic and natural contributions (e.g., DMS derived sulfate AOD and biomass
170 burning AOD, among others). The AOD distributions clearly show several hotspots
171 representing well-known industrial pollution regions (e.g., East and South Asia, Western
172 Europe, and eastern US) and biomass burning regions (e.g., equatorial Africa in DJF,
173 South America and southern Africa in JJA and SON). In **Table 2**, the global annual mean
174 AOD is 0.0335 ± 0.0134 (average \pm standard deviation of the 9 models), $0.0108 \pm$
175 0.0047 , and 0.0022 ± 0.0024 for SO_4 , POM, and BC, respectively. Clearly AOD shows
176 large model diversity with the standard deviation equivalent to about half of the multi-
177 model average. These global annual means are lower than those from multiple model
178 simulations with harmonized emissions under the framework of the Aerosol Comparisons
179 between Observations and Models (AeroCom) [Schulz *et al.*, 2006] by 10%, 28%, and
180 8% for sulfate, POM, and BC, respectively.

181

182 **Figure 3(a)** shows the 9-model median AOD for sulfate, POM, and BC combined as
183 derived from the SR1 baseline simulations and its comparisons with anthropogenic AOD
184 derived from MODIS over-ocean measurements using two different methods described
185 by Yu *et al.* [2009] (**Figure 3b**, denoted as MODIS-YU09) and Bellouin *et al.* [2008]
186 (**Figure 3c**, denoted as MODIS-BE08). MODIS-YU09 anthropogenic AOD is derived
187 from MODIS over-ocean retrievals of AOD and fine-mode fraction (FMF) using the
188 representative FMF values for individual aerosol types, which are determined from
189 MODIS observations in selected regions where the specific aerosol type predominates
190 [Yu *et al.*, 2009]. MODIS-BE08 is derived from the same MODIS measurements, but

191 with the use of prescribed, in situ measurement-based thresholds of FMF for different
192 aerosol types (which are different from those derived from MODIS observations as in Yu
193 et al., 2009) aided by the satellite observed absorbing aerosol index to separate
194 anthropogenic aerosol from mineral dust and sea salt [Bellouin et al., 2008]. Deriving
195 anthropogenic AOD from satellite measurements over land is not currently feasible. As
196 shown in Figure 3, anthropogenic AOD of MODIS-YU09 is generally larger than
197 MODIS-BE08 AOD in northern hemispheric mid-latitudes. In the tropics, MODIS-BE08
198 AOD is somewhat higher than MODIS-YU09. Except for trans-Pacific transport in
199 spring, the cross-ocean transport from major industrial pollution and biomass burning
200 regions is generally more extensive in the HTAP model simulations than both MODIS-
201 based estimates. In particular, the models simulated significant cross-Atlantic transport of
202 tropical African smoke to South America in boreal winter, which is not clearly seen in the
203 MODIS-based estimates. **Figure 4** further compares zonal variations of HTAP seasonal
204 AOD for the sulfate, POM and BC mixture against that of the MODIS anthropogenic
205 AOD over the ocean in mid-latitudes (20-60°N) of the Northern Hemisphere, where the
206 major intercontinental transport paths occur. Significant regional and seasonal differences
207 exist between the HTAP models and MODIS observations and between MODIS-YU09
208 and MODIS-BE08. In the North Atlantic, the MODIS anthropogenic AOD from both
209 methods is often near the low bound of 9 HTAP models. In the North Pacific, MODIS-
210 YU09 anthropogenic AOD generally agrees well with the median of HTAP models. On
211 the other hand, MODIS-BE08 is consistently lower than MODIS-YU09 and generally
212 entails the low bound of the HTAP model simulations, particularly in the northeastern
213 Pacific. The differences between the two MODIS-based estimates of anthropogenic AOD

214 result from the differences in specifics of the approaches, as discussed in Yu et al.
215 [2009]. The pronounced differences between the two MODIS-based estimates of
216 anthropogenic AOD manifest the urgent need to develop independent approaches based
217 on other satellite measurements, and more importantly, to conduct in situ measurements
218 of anthropogenic AOD over large scales [Yu et al., 2009].

219

220 **2.3 Estimate of the aerosol direct radiative forcing**

221 Because the aerosol direct radiative forcing or the aerosol optical properties (i.e., single-
222 scattering albedo and asymmetry factor) for calculating the forcing are not archived under
223 the HTAP S/R experiment protocol, we estimate here the aerosol DRF for each model
224 and component (i.e., sulfate, POM, or BC) as follows:

$$225 \quad \text{DRF}_i(x, y, t) = \text{AOD}_i(x, y, t) \cdot \text{NDRF}_i(x, y, t) \quad (i = \text{SO}_4, \text{POM}, \text{and BC}) \quad (1)$$

226 where x , y , and t represents longitude, latitude, and month, respectively, and NDRF is
227 the normalized DRF with respect to AOD at 550 nm [Zhou et al., 2005]. In this study we
228 derive monthly average NDRF_{*i*} over each model grid cell by dividing the DRF by the
229 AOD, using 2001 monthly average AOD and direct radiative forcing calculated from the
230 Goddard Chemistry Aerosol Radiation and Transport (GOCART) model [Chin et al.,
231 2002]. We then apply this NDRF_{*i*} to the monthly average component AOD_{*i*} from the
232 other models in the HTAP S/R experiments. We also estimate DRF for an external
233 mixture of SO₄, POM and BC by simply summing up the DRF for individual
234 components. Note that RF for an internal mixture could differ significantly from that for
235 an external mixture [Jacobson, 2001; Chung and Seinfeld, 2002]. Although DRF does
236 not increase with AOD in a fully linear manner over the whole range of AOD, the use of

237 the above linear formula to derive DRF and its change in response to a 20% reduction of
238 emissions would not introduce large uncertainties with respect to regional differences in
239 DRF [Zhou et al., 2005; Anderson et al., 2005].

240

241 The GOCART model currently prescribes particle size distributions and refractive indices
242 for individual components based on the Optical Properties of Aerosols and Clouds
243 (OPAC) database [Hess et al., 1998]. Aerosol properties such as AOD, single scattering
244 albedo, and asymmetry factor are then calculated using the Mie code [Chin et al., 2002,
245 2009]. These aerosol optical properties along with surface albedos and cloud fields from
246 the Goddard Earth Observing System (GEOS) Data Assimilation System - Version 4 are
247 then used to drive the NASA Goddard radiative transfer model [Chou et al., 1998]. The
248 time step for the radiative transfer calculations is 30 min, which can adequately capture
249 the dependence of DRF on solar zenith angle [Yu et al., 2004]. For a specific component
250 (e.g., SO₄, POM, or BC), DRF is calculated as the difference of net downward radiative
251 flux between a radiative transfer calculation including all aerosol components and one
252 with the specific component excluded. This DRF is therefore different from the DRF
253 estimated in Forster et al. [2007], where the reference is pre-industrial aerosols. In this
254 study, the GOCART DRF is calculated for solar radiation only and averaged over a 24-
255 hour period. GOCART calculations of DRF have been evaluated against remote sensing
256 measurements and other model simulations [e.g., Yu et al., 2004; Yu et al., 2006].

257

258 **Table 3** lists the annual mean NDRF in the four defined regions and globally. For purely
259 scattering SO₄, NDRF is nearly the same at the top of atmosphere (TOA) and at the

260 surface. Because POM is partially absorbing in the UV range [Chin et al., 2009], the
261 surface NDRF is more negative than the TOA NDRF. BC aerosol is strongly absorbing
262 over the whole solar spectrum, thus its TOA forcing is positive (i.e., TOA warming),
263 while the surface forcing is strongly negative (i.e., surface cooling). Clearly BC aerosol is
264 much more effective in interacting with solar radiation than SO₄ and POM, although it is
265 typically associated with lower AODs. For a specific component, the difference in NDRF
266 among regions is generally within 20-30%, due to the combined effects of differences in
267 solar zenith angle, surface albedo, and cloud fields [Yu et al., 2006]. The global annual
268 mean all-sky TOA NDRF is -24.2, -30.0, and +85.9 Wm⁻²τ⁻¹ for SO₄, POM, and BC,
269 respectively. These values fall within the ranges reported in the literature, i.e., -10 ~ -32
270 Wm⁻²τ⁻¹ for SO₄, -5 ~ -38 Wm⁻²τ⁻¹ for POM, and +22 ~ +216 Wm⁻²τ⁻¹ for BC [CCSP,
271 2009].

272

273 To apply the GOCART-based monthly NDRF_i to the HTAP models, we regrid the
274 component AOD_i from each model to a unified spatial resolution of 2°x2.5° and use eq.
275 (1) to estimate the corresponding DRF_i. For the SR1 experiment and on a global and
276 annual basis, the 9 models give the mean all-sky TOA DRF of -0.67 ± 0.28, -0.26 ± 0.13,
277 and +0.22 ± 0.13 Wm⁻² for SO₄, POM, and BC, respectively. Correspondingly, the
278 respective DRF at the surface and in all-sky (including both cloudy and cloud-free)
279 condition is -0.64 ± 0.26, -0.37 ± 0.19, and -0.43 ± 0.22 Wm⁻². When the anthropogenic
280 fraction of AOD, e.g., 55%, 53%, and 100% respectively for SO₄, POM, and BC on a
281 global and annual average basis [Schulz et al., 2006] is considered, our DRF estimates
282 shown above are in good agreement with anthropogenic TOA DRF of -0.35 ± 0.15 Wm⁻²

283 (SO₄), $-0.13 \pm 0.05 \text{ Wm}^{-2}$ (POM), and $+0.25 \pm 0.09 \text{ (BC) Wm}^{-2}$ reported by *Schulz et al.*
284 *[2006]*. The aerosol direct radiative forcing exhibits large regional and seasonal
285 variations, as shown in **Figure 5** for the all-sky DRF and for the external mixture of SO₄,
286 POM, and BC, as derived from the 9-model SR1 simulations. Over major industrial
287 pollution regions in northern hemispheric mid-latitudes, aerosol DRF can be as large as -
288 6 Wm^{-2} at TOA and -25 Wm^{-2} at the surface. The forcing is greater in JJA and MAM
289 than in DJF and SON. Similar magnitudes of DRF are seen in the tropics where biomass
290 burning smoke is dominant. The seasonal variations of DRF reflect the peak seasons of
291 biomass burning, e.g., DJF in the Sahel and JJA and SON in southern Africa and South
292 America.

293

294 We note that the use of GOCART-based NDRF is likely to understate the model diversity
295 in DRF, in comparison to that derived from full radiative transfer calculations by
296 participating models. Although other aerosol models currently use the OPAC to
297 characterize aerosol microphysical and optical properties just like GOCART, models can
298 differ substantially in aerosol vertical distributions, meteorological fields (such as relative
299 humidity, cloud distributions, and surface albedos), and radiative transfer schemes. These
300 differences combined may lead to large model differences in DRF. This could
301 particularly be the case for all-sky TOA DRF by BC, which depends strongly on the
302 vertical distributions of aerosol and clouds, as evidenced by the reported wide range of
303 DRF *[CCSP, 2009]*.

304

305 **3. Influences of regional anthropogenic emission reductions on AOD** 306 **and DRF**

307 In this section we present how the 20% reduction of regional anthropogenic emissions
308 changes AOD and DRF by analyzing differences between a set of SR6 experiments
309 (SR6NA, SR6EU, SR6EA, and SR6SA) and the SR1 experiment. We examine first the
310 changes in global mean AOD and DRF and then the spatial extents of AOD and DRF
311 changes resulting from regional anthropogenic emission reductions. The relative roles of
312 ICT and regional emissions are assessed with a concept of the relative annual
313 intercontinental response (RAIR) (as defined in HTAP, 2010). For the reasons discussed
314 earlier in 2.2, we exclude ECHAM5 results in the analysis of AOD and DRF magnitude.
315 Because RAIR is less sensitive to water optical depth than AOD is, we include ECHAM5
316 results in the RAIR analysis.

317

318 **3.1. Global mean**

319 Just as aerosol radiative forcing varies regionally, the effects of changes in emissions of
320 aerosols and their precursors on global mean DRF also varies with region. **Tables 4** and
321 **5** list respectively changes of global annual average AOD and all-sky DRF in response to
322 the 20% reduction of anthropogenic emissions in the four HTAP anthropogenic source
323 regions. The combined impact of the 20% reduction of emissions in all of the four
324 regions is to decrease AOD and DRF by about 9%, 4%, and 10% for sulfate, POM, and
325 BC, respectively. Relative contributions from individual regions vary considerably. For
326 sulfate, the change of global average AOD and DRF due to the reduction of SO₂
327 emissions in South Asia is substantially smaller than that due to the emission reductions

328 from the other regions. This is mainly because SO₂ emissions in the SA region are much
329 smaller than those in other regions (see Figure 1). For POM, the reductions of global
330 mean AOD and DRF due to the regional emission reduction are generally consistent with
331 regional differences in primary POM emissions. For BC, the reduction of emissions in
332 East Asia makes the largest contribution to the change of global average DRF, mainly
333 because of the highest BC emissions among the four regions. For the external mixture of
334 SO₄, POM, and BC, the 20% reductions in the anthropogenic emissions in the four
335 regions collectively yield the respective reductions of 0.0035, 45.5 mWm⁻², (1 mWm⁻² =
336 10⁻³ Wm⁻²) and 104.1 mWm⁻² for global mean AOD, all-sky DRF at TOA and at the
337 surface, which represents respectively about 8%, 6% and 7% reduction from the baseline
338 simulation. Note that uncertainties are larger than given by the standard deviation in
339 Table 5, due to the use of NDRF from a single model, as discussed earlier.

340

341 Will the same amount of emission reduction in different regions introduce the same
342 change in global mean aerosol radiative forcing? To address this question, we calculate
343 the forcing efficiency with respect to emissions by normalizing the global annual mean
344 DRF difference between the SR6 and SR1 runs by the change (20%) in regional
345 emissions for each model, as shown in **Table 6**. For SO₄ and POM, we use the emissions
346 for SO₂ and primary POM respectively to calculate the forcing efficiency. These derived
347 forcing efficiency numbers should be considered as rough estimates, because some
348 models with fully coupled chemistry include changes of SO₄ resulting from the
349 reductions of other anthropogenic emissions (Fry et al., 2012) and a fraction of POM is
350 secondary aerosol formed from volatile organic carbon emissions. Clearly the forcing

351 efficiency for BC is an order of magnitude higher than that for SO₄ and POM, suggesting
352 that BC emission control is a candidate for producing a large, near-term cooling that
353 counters the warming of greenhouse gases. Despite wide model differences in the
354 absolute value of forcing efficiency, several regional dependences appear to be rather
355 robust among the models. As shown in **Figure 6**, all eight models consistently yield a
356 smaller sulfate forcing efficiency for EA emissions than for EU emissions, which is
357 consistent with the oxidant limitation in EA that reduces the efficiency of SO₂-to-sulfate
358 transformation [Koch *et al.*, 2007]. The models also consistently give the largest BC
359 forcing efficiency for EU emissions. These results may have important implications for
360 regional emission controls and their influences on global climate, which will be discussed
361 in section 4.

362

363 **3.2. Spatial extents and the role of ICT**

364 The spatial extents of the AOD and DRF due to the reduction of regional emissions and
365 the role of aerosol ICT are revealed by differencing SR6 and SR1 experiments. **Figure 7**
366 shows the 9-model annual average changes of AOD and all-sky DRF by the external
367 mixture of SO₄, POM, and BC, resulting from the 20% reduction of anthropogenic
368 emissions over the four regions. Clearly emissions from North America, Europe, and East
369 Asia exert significant DRF on intercontinental and even hemispheric scales. Emissions
370 from South Asia have relatively small impacts mainly over the Indian Ocean and the
371 tropical Pacific. The influences of regional emission reduction on AOD and DRF also
372 depend on season. As an example, **Figure 8** shows seasonal variations of changes of the
373 all-sky surface DRF between SR1 and SR6. Similar seasonal variations occur for AOD,

374 all-sky DRF at TOA and clear-sky DRF, which will not be discussed separately. For
375 North America, Europe, and East Asia, the 20% reduction of emissions in each region
376 decreases the direct forcing (i.e., less negative) by a larger amount and over more
377 extensive areas in summer and spring than in winter and fall. For comparison, the
378 influence of the 20% reduction of emissions in South Asia shows relatively small
379 seasonal variations.

380

381 To quantify the role of aerosol ICT in affecting regional climate forcing, we adopt a
382 concept of the RAIR as defined in HTAP [2010]. For AOD, RAIR in a receptor region i
383 is expressed as follows:

384

$$385 \quad RAIR_i = \frac{\sum_j \delta AOD_{ji}}{\delta AOD_{ii} + \sum_j \delta AOD_{ji}} \quad (j \neq i)$$

386

387 where index j represents a source region. δAOD_{ii} represents a change of AOD in the
388 receptor/domestic region i due to the emission reduction in the region itself and δAOD_{ji}
389 represents a change of AOD in the receptor i induced by the emission reduction in a
390 source region j outside of the receptor (or foreign region). Similarly, RAIR can be
391 defined for DRF, near-surface concentration, and surface deposition. By definition, RAIR
392 in a receptor region represents the percentage contribution of the intercontinental
393 transport of foreign emissions relative to the sum of foreign and domestic emissions.

394

395 We calculate the RAIR for AOD and DRF for individual models and then obtain multi-
396 model averages, as shown respectively in **Figure 9** and **10** with the columns representing

397 10-model (including ECHAM5) average and error bars indicating ± 1 standard deviation
398 of the model simulations. Clearly values of RAIR depend on both region and component.
399 For all regions and components, the import from intercontinental transport is significant
400 but local emissions remain the main contributor, with RAIR ranging from 10 to 30%.
401 South Asia is most influenced by the import of sulfate aerosol, and North America is
402 most influenced by the import of BC, followed by POM. For sulfate, POM, and BC
403 combined, South Asia DRF is most strongly influenced by foreign sources, and North
404 America and Europe is the least. These rankings also reflect the strength of local
405 emissions relative to world emissions, as discussed in section 2. Interestingly, RAIR
406 values for AOD and DRF of sulfate (10-30%) are consistently smaller than that for
407 aerosol column loading (i.e., 24-37%) [see Table 4.4 in HTAP 2010]. For POM, RAIR
408 values (16-18%) for AOD and DRF in NA and EU are also somewhat smaller than the
409 corresponding RAIR values (21-23%) for the column mass loading. These differences
410 probably stem from transported sulfate and POM aerosols experiencing lower relative
411 humidity at high altitude (resulting in lower optical depth) than local aerosols, which
412 generally remain at lower altitudes. Finally, model variability is very large, highlighting
413 the significant uncertainties in modeling aerosol processes.

414

415 The contributions of emission reductions in a receptor region depend on source regions.
416 **Table 7** lists the response of annual mean AOD and all-sky DRF in receptor regions to a
417 20% reduction of anthropogenic emissions in the four source regions. Here we combine
418 SO₄ and POM together, in which SO₄ makes a dominant contribution of 69-94%,
419 depending on regions. BC is listed separately from the SO₄ and POM combined, because

420 strongly absorbing BC has different effects on solar radiation than do weakly absorbing
421 sulfate and organic matter. Not surprisingly, the influences on AOD and DRF from the
422 reduction of domestic emissions is about an order of magnitude larger than from any
423 foreign source region. Foreign source regions also differ in contributing to the total
424 import for a specific receptor region. The intercontinental transport of EA emissions
425 accounts for the largest fraction of total import in NA, i.e., 60% and 70% for SO₄+POM,
426 and BC, respectively. The NA emissions make the largest contribution (57%) to the total
427 import of SO₄+POM into EU. For BC aerosols imported to EU, on the other hand, the EA
428 contribution of 45% exceeds the NA contribution of 35%, presumably because of much
429 higher BC emissions in EA. The imported BC to EA comes mostly (65%) from SA,
430 followed by those from EU (e.g., 30%). For the import of SO₄+POM to EA, SA and EU
431 emissions make quite comparable contributions, which is more than a factor of 3 larger
432 than NA emissions. In SA, the imported SO₄+POM is significant, with RAIR of 24%, of
433 which 66% comes from EU, followed by 28% from EA. For BC aerosols in SA, the
434 import from EA and EU emissions contributes more or less equally (e.g., 48% and 44%).
435

436 Our multi-model estimates of the relative contributions of local emissions and ICT import
437 are generally consistent with results in literature. In NA, we estimate that local emissions
438 account for about 81% of anthropogenic AOD, which is higher than 66% estimated by a
439 modeling study [Leibensperger *et al.*, 2012]. This difference would be narrowed if
440 emissions in regions other than the four defined regions of this study are taken into
441 account. Yu *et al.* [2012a] estimate based on satellite measurements that the imported
442 pollution via trans-Pacific transport results in a clear-sky TOA direct forcing of -0.49

443 Wm^{-2} over NA, which accounts for about 11.5% of total anthropogenic aerosol direct
444 forcing. For comparison, our estimated contribution by ICT import to the direct forcing
445 over NA is 14.7% in this study. The BC fractional contributions from different source
446 regions as estimated in this study also agree well with a model estimate [*Reddy and*
447 *Boucher, 2009*, referred to as RB09]. RB09 estimated that over North America, emissions
448 from East and South Asia contribute to 18% and 6% of the total BC burden, respectively,
449 which are somewhat smaller than our corresponding estimate of 23% and 8%. The
450 contribution of North America emissions to BC burden in Europe was estimated at 5% in
451 RB09, which is also somewhat smaller than our estimated 8%. RB09 estimated that the
452 local BC emissions over South and East Asia accounts for more than 80% of the BC
453 burden, which agrees well with our estimate of 82% and 84%. These comparisons show
454 how the estimated significance of ICT import in this study agrees broadly with results in
455 the literature, as these studies have defined source regions somewhat differently.

456

457 **4. Conclusions and discussion**

458 We have assessed impacts of a 20% reduction of anthropogenic emissions in North
459 America, Europe, East Asia, and South Asia on the aerosol optical depth and direct
460 radiative forcing by using results from 10 global chemical transport models. On the basis
461 of the multi-model average, a 20% reduction of anthropogenic emissions in the four
462 regions combined lowers the global mean AOD and DRF by about 9%, 4%, and 10% for
463 sulfate, organic matter, and black carbon aerosol, respectively. Despite the considerable
464 model-to-model differences in the magnitude of forcing efficiency (direct radiative
465 forcing per unit emissions), the models appear to consistently give a lower sulfate forcing

466 efficiency for SO₂ emissions from EA than that from EU, and the largest BC forcing
467 efficiency for the EU emissions. These results may suggest that reducing BC emissions in
468 EU would be relatively the most efficient way to mitigate the warming effect of BC
469 aerosol, not considering cost and feasibility. However, a larger potential for BC
470 reductions is available in East Asia. Reducing SO₂ emissions decreases the cooling effect
471 of aerosols that counteracts the greenhouse warming; but the impact of reducing EA SO₂
472 is less pronounced (ca. 25%) than reducing EU, NA, or SA SO₂ by the same amount.
473 However, such implications need to be further explored by taking into account a variety
474 of aerosol impacts on climate through modifying cloud microphysics, changing
475 atmospheric circulations, and altering the snow albedo. The air quality implication of
476 any emission control should also be considered.

477

478 Our multi-model simulations of source-receptor relationships show that the impacts of
479 the regional emission reductions are not confined to the region itself because of aerosol
480 intercontinental transport. On an annual basis, intercontinental transport accounts for 10-
481 30% of the overall AOD or DRF in a receptor region, compared to the influence of both
482 regional emissions and intercontinental transport, depending on regions and species.

483 While South Asia is most influenced by import of sulfate aerosol from Europe, North
484 America is most influenced by import of black carbon aerosol from East Asia. Given that
485 BC deposition may accelerate the melting of snow in the Sierra Nevada and cause water
486 supply shortage in summer in the western U.S. [*Hadley et al., 2010*], the region may
487 likely benefit from a future control of BC emissions in Asia.

488

489 The multi-model assessment shows large differences between models in the impacts of
490 emission reductions and the role of intercontinental transport, which highlights a need for
491 improving models and developing observational databases for evaluating and
492 constraining models. Quantifying anthropogenic AOD distributions from satellite
493 measurements remains challenging, in particular over land. Current estimates of
494 anthropogenic AOD based on total AOD and fine-mode fraction measurements from
495 MODIS are only feasible over ocean and subject to large uncertainties [Yu et al., 2009;
496 Bellouin et al., 2005, 2008]. Such an estimate would be better constrained by a
497 synergistic use of aerosol microphysical measurements as provided by other satellite
498 sensors [Yu et al., 2012b and references therein]. Large-scale in situ measurements of
499 anthropogenic AOD will be essential for evaluating satellite observations and model
500 simulations. From the perspective of model improvements, efforts should focus on not
501 only emission inventories [Textor et al., 2007] but also a variety of atmospheric
502 processes that determine the atmospheric evolution of aerosols, such as parameterization
503 of dry deposition and wet scavenging [Prospero et al., 2011]. Given that the aerosol
504 intercontinental transport and its influences involve a wide span of scales, it is necessary
505 to develop modeling systems that link the local, regional, intercontinental, and global
506 scales.

507

508 **Acknowledgements:** HY was supported by NASA grant NNX11AH66G, managed by
509 Richard Eckman. MC and HB were supported by NASA Modeling, Analysis, and
510 Prediction program managed by David Considine. NB thanks Shekar Reddy, formerly
511 with the Met Office Hadley Centre, for carrying out the HadGEM2 simulations. We are

512 grateful to many colleagues, including Frank Dentener and Bill Collins for helpful
513 comments. The HTAP experiments used in this study were organized by Martin Schultz,
514 Arlene Fiore, Kees Cuvelier, Frank Dentener, Christiane Textor, Terry Keating, and
515 Andre Zuber.

516

517

518 **References**

519 Albrecht, B. (1989), Aerosols, cloud microphysics, and fractional cloudiness, *Science*,
520 **245**, 1227-1230.

521 Anderson, T.L., et al. (2005), An "A-Train" strategy for quantifying direct aerosol
522 forcing of climate, *Bull. Am. Met. Soc.*, **86**, 1795-1809.

523 Bellouin, N., O. Boucher, J. Haywood, and M. S. Reddy (2005), Global estimate of
524 aerosol direct radiative forcing from satellite measurements, *Nature*, **438**, 1138-
525 1141, doi:10.1038/nature04348.

526 Bellouin, N., J. Rae, A. Jones, C. Johnson, J. Haywood, and O. Boucher (2011), Aerosol
527 forcing in the Climate Model Intercomparison Project (CMIP5) simulations by
528 HadGEM2-ES and the role of ammonium nitrate, *J. Geophys. Res.*, **116**, D20206,
529 doi:10.1029/2011JD016074.

530 Bellouin, N., A. Jones, J. Haywood, and S. A. Christopher (2008), Updated estimate of
531 aerosol direct radiative forcing from satellite observations and comparison against
532 the Hadley Centre climate model, *J. Geophys. Res.*, **113**, D10205,
533 doi:10.1029/2007JD009385.

534 Bian, H., M. Chin, J. M. Rodriguez, H. Yu, J. E. Penner, and S. Strahan (2009),
535 Sensitivity of aerosol optical thickness and aerosol direct radiative effect to relative
536 humidity, *Atmos. Chem. Phys.*, **9**, 2375-2386, doi:10.5194/acp-9-2375-2009.

537 CCSP (2009), Atmospheric Aerosol Properties and Climate Impacts, A Report by the
538 *U.S. Climate Change Science Program and the Subcommittee on Global Change*

539 *Research*. [Mian Chin, Ralph A. Kahn, and Stephen E. Schwartz (eds.)]. National
540 Aeronautics and Space Administration, Washington, D.C., USA, 128 pp.

541 Chin, M., et al. (2002), Tropospheric aerosol optical thickness from the GOCART model
542 and comparisons with satellite and sun photometer measurements, *J. Atmos., Sci.*,
543 **59**, 461–483.

544 Chin, M., T. Diehl, P. Ginoux, and W. Malm (2007), Intercontinental transport of
545 pollution and dust aerosols: implications for regional air quality, *Atmos. Chem.*
546 *Phys.*, **7**, 5501-5517, doi:10.5194/acp-7-5501-2007.

547 Chin, M., T. Diehl, O. Dubovik, T. F. Eck, B. N. Holben, A. Sinyuk, and D. G. Streets
548 (2009), Light absorption by pollution, dust and biomass burning aerosols: A global
549 model study and evaluation with AERONET data. *Ann. Geophys.*, **27**, 3439-3464.

550 Chou, M. D., M. J. Suarez, C. H. Ho, M. M. H. Yan, and K. T. Lee (1998),
551 Parameterizations for cloud overlapping and shortwave single-scattering properties
552 in the Goddard GCM, *J. Climate*, **11**, 201–214.

553 Chung, S. H., and J. H. Seinfeld (2002), Global distribution and climate forcing of
554 carbonaceous aerosols, *J. Geophys. Res.*, **107**, 4407, doi:10.1029/2001JD001397.

555 Clarke, A., and V. Kapustin (2010), Hemispheric aerosol vertical profiles: Anthropogenic
556 impacts on optical depth and cloud nuclei, *Science*, **329**, 1488-1492.

557 Dirksen, R. J., K. F. Boersma, J. de Laat, P. Stammes, G. R. van der Werf, M. Val
558 Martin, and H. M. Kelder (2009), An aerosol boomerang: Rapid around-the-world
559 transport of smoke from the December 2006 Australian forest fires observed from
560 space, *J. Geophys. Res.*, **114**, D21201, doi:10.1029/2009JD012360.

561 Fiore, A. M., et al. (2009), Multimodel estimates of intercontinental source-receptor
562 relationships for ozone pollution, *J. Geophys. Res.*, **114**, D04301,
563 doi:10.1029/2008JD010816.

564 Fischer, E. V., D. A. Jaffe, N. A. Marley, J. S. Gaffney, and A. Marchany-Rivera (2010),
565 Optical properties of aged Asian aerosols observed over the U.S. Pacific Northwest,
566 *J. Geophys. Res.*, **115**, D20209, doi:10.1029/2010JD013943.

567 Forster, P., et al. (2007), Changes in Atmospheric Constituents and Radiative Forcing.
568 *Climate Change 2007: The Physical Scientific Basis*, Cambridge University Press,
569 United Kindom and New York, NY, USA.

570 Fry, M. M., et al. (2012), The influence of ozone precursor emissions from four world
571 regions on tropospheric composition and radiative climate forcing, *J. Geophys. Res.*,
572 **117**, D07306, doi:10.1029/2011JD017134.

573 Gunn, R., and B. B. Philips (1957), An experimental investigation of the effect of air
574 pollution on the initiation of rain, *J. Meteorol.*, **14**, 272-280.

575 Hadley, O. L., V. Ramanathan, G. R. Carmichael, Y. Tang, C. E. Corrigan, G. C.
576 Roberts, and G. S. Mauger (2007), Trans-Pacific transport of black carbon and fine
577 aerosols ($D < 2.5 \mu\text{m}$) into North America, *J. Geophys. Res.*, **112**, D05309,
578 doi:10.1029/2006JD007632.

579 Hadley, O. L., C. E. Corrigan, T. W. Kirchstetter, S. Cliff, and V. Ramanathan, Measured
580 black carbon deposition on the Sierra Nevada snow pack and implication for snow
581 pack retreat. *Atmos. Chem. Phys.*, **10**, 7505-7513, 2010.

582 Hauglustaine, D. A., F. Hourdin, S. Walters, L. Jourdain, M.-A. Filiberti, J.-F.
583 Larmarque, and E. A. Holland (2004), Interactive chemistry in the Laboratoire de
584 Météorologie Dynamique general circulation model: description and background
585 tropospheric chemistry evaluation, *J. Geophys. Res.*, **109**, D04314,
586 doi:10.1029/3JD003957.

587 Heald, C. L., et al. (2006), Transpacific transport of Asian anthropogenic aerosols and its
588 impact on surface air quality in the United States, *J. Geophys. Res.*, **111**, D14310,
589 doi:10.1029/2005JD006847.

590 Hess, M., P. Koepke, and I. Schult (1998), Optical Properties of Aerosols and Clouds:
591 The Software Package OPAC, *Bull. Amer. Meteor. Soc.*, **79**, 831–844.

592 HTAP (2010), *Hemispheric Transport of Air Pollution 2010 - Part A: Ozone and*
593 *Particulate Matter*, Air Pollution Studies No. 17, edited by Frank Dentener, Terry
594 Keating, and Hajime Akimoto, United Nations, New York and Geneva.

595 Jacobson, M. Z. (2001), Strong radiative heating due to the mixing state of black carbon
596 in atmospheric aerosols, *Nature*, **409**, 695-697.

597 Kinne, S., et al. (2006), An AeroCom initial assessment – optical properties in aerosol
598 component modules of global models, *Atmos. Chem. Phys.*, **6**, 1815-1834,
599 doi:10.5194/acp-6-1815-2006.

600 Koch, D., G. A. Schmidt, and C. Field (2005), Sulfur, sea salt and radionuclide aerosols
601 in GISS, ModelE, *J. Geophys. Res.*, **111**, D06206, doi:10.1029/2004JD005550.

602 Koch, D., T. C. Bond, D. G. Streets, N. Unger, and G. R. van der Werf (2007), Global
603 impacts of aerosols from particular source regions and sectors, *J. Geophys. Res.*,
604 **112**, D02205, doi:10.1029/2005JD007024.

605 Leibensperger, E. M., et al. (2012), Climatic effects of 1950-2050 changes in US
606 anthropogenic aerosols – Part 1: Aerosol trends and radiative forcing, *Atmos. Chem.*
607 *Phys.*, **12**, 3333-3348.

608 Li, Z., K.-H. Lee, Y. Wang, J. Xin, and W.-M. Hao (2010), First observation-based
609 estimates of cloud-free aerosol radiative forcing across China, *J. Geophys. Res.*,
610 **115**, D00K18, doi:10.1029/2009JD013306.

611 McCormick, R. A., and J. H. Ludwig (1967), Climate modification by atmospheric
612 aerosols, *Science*, **156**, 1358-1359.

613 Pfister, G. G., P. G. Hess, L. K. Emmons, P. J. Rasch, and F. M. Vitt (2008), Impact of
614 the summer 2004 Alaska fires on top of the atmosphere clear-sky radiation fluxes, *J.*
615 *Geophys. Res.*, **113**, D02204, doi:10.1029/2007JD008797.

616 Pozzoli, L, I. Bey, S. Rast, M. G. Schultz, P. Stier, and J. Feichter (2008a), Trace gas and
617 aerosol interactions in the fully coupled model of aerosol-chemistry-climate
618 ECHAM5-HAMMOZ: 1. Model description and insights from the spring 2001
619 TRACE-P experiment, *J. Geophys. Res.*, **113**, D07308,
620 doi:10.1029/2007/JD009007.

621 Pozzoli, L, I. Bey, S. Rast, M. G. Schultz, P. Stier, and J. Feichter (2008b), Trace gas and
622 aerosol interactions in the fully coupled model of aerosol-chemistry-climate
623 ECHAM5-HAMMOZ: 2. Impact of heterogeneous chemistry on the global aerosol
624 distribution, *J. Geophys. Res.*, **113**, D07309, doi:10.1029/2007/JD009008.

625 Prospero, J. M., D. L. Savoie, and R. Arimoto (2003), Long-term record of nss-sulfate
626 and nitrate in aerosols on Midway Island, 1981-2000: Evidence of increased (now
627 decreasing?) anthropogenic emissions from Asia, *J. Geophys. Res.*, **108**, 4019,
628 doi:10.1029/2001JD001524.

629 Prospero, J. M., W. M. Landing, and M. Schulz (2010), African dust deposition to
630 Florida: Temporal and spatial variability and comparisons to models, *J. Geophys.*
631 *Res.*, **115**, D13304, 10.1029/2009jd012773.

632 Ramanathan, V., et al. (2001), Indian Ocean Experiment: An integrated analysis of the
633 climate forcing and effects of the great Indo-Asian haze, *J. Geophys. Res.*, **106**,
634 28,371–28,398, doi:10.1029/2001JD900133.

635 Ramanathan, V., et al. (2007), Atmospheric brown clouds: Hemispherical and regional
636 variations in long-range transport, absorption, and radiative forcing, *J. Geophys.*
637 *Res.*, **112**, D22S21, doi:10.1029/2006JD008124.

638 Reddy, M. S., and O. Boucher (2009), Climate impacts of black carbon emitted from
639 energy consumption in the world's regions. *Geophys. Res. Lett.*, **34**, L11802,
640 doi:10.1029/2006GL028904.

641 Rotman, D. A., et al. (2004), IMPACT, the LLNL 3-D global atmospheric chemical
642 transport model for the combined troposphere and stratosphere: Model description
643 and analysis of ozone and other trace gases, *J. Geophys. Res.*, **109**, D04303,
644 doi:10.1029/2002JD003155.

645 Rudich, Y., Y. J. Kaufman, U. Dayan, H. Yu, and R. G. Kleidman (2008), Estimation of
646 transboundary transport of pollution aerosols by remote sensing in the eastern
647 Mediterranean, *J. Geophys. Res.*, **113**, D14S13, doi:10.1029/2007JD009601.

648 Satheesh, S. K., and V. Ramanathan (2000), Large differences in tropical aerosol forcing
649 at the top of atmosphere and Earth's surface, *Nature*, **405**, 60-63.

650 Schulz, M., et al. (2006), Radiative forcing by aerosols as derived from the AeroCom
651 present-day and pre-industrial simulations, *Atmos. Chem. Phys.*, **6**, 5225-5246,
652 doi:10.5194/acp-6-5225-2006.

653 Schulz, M. (2007), Constraining model estimates of the aerosol radiative forcing, Thèse
654 d'Habilitation à Diriger des Recherches, Université Pierre et Marie Curie, Paris
655 VI .

656 Shindell, D. T., et al. (2006), Simulations of preindustrial, present-day, and 2100
657 conditions in the NASA GISS composition and climate model G-PUCCINI, *Atmos.*
658 *Chem. Phys.*, **6**, 4427-4459, doi:10.5194/acp-6-4427-2006.

659 Shindell, D., et al. (2008a), Climate forcing and air quality change due to regional
660 emissions reductions by economic sector, *Atmos. Chem. Phys.*, **8**, 7101-7113.

661 Shindell, D., et al. (2008b), Multimodel projections of climate change from short-lived
662 emissions due to human activities. *J. Geophys. Res.*, **113**, D11109,
663 doi:10.1029/2007JD009152.

664 Shindell, D., et al. (2008c), A multi-model assessment of pollution transport to the Arctic.
665 *Atmos. Chem. Phys.*, **8**, 5353-5372.

666 Takemura, T., T. Nozawa, S. Emori, T. Y. Nakajima, and T. Nakajima (2005),
667 Simulation of climate response to aerosol direct and indirect effects with aerosol
668 transport-radiation model. *J. Geophys. Res.*, **110**, D02202,
669 doi:10.1029/2004JD005029.

670 Textor, C., et al. (2006), Analysis and quantification of the diversities of aerosol life
671 cycles within AeroCom, *Atmos. Chem. Phys.*, **6**, 1777-1813, doi:10.5194/acp-6-
672 1777-2006.

673 Textor, C., et al. (2007), The effect of harmonized emissions on aerosol properties in
674 global models – an AeroCom experiment, *Atmos. Chem. Phys.*, **7**, 4489-4501.

675 Twomey, S. (1977), The influence of pollution on the shortwave albedo of clouds, *J.*
676 *Atmos. Sci.*, **34**, 1149-1152.

677 VanCuren, R. A. (2003), Asian aerosols in North America: Extracting the chemical
678 composition and mass concentration of the Asian continental aerosol plume from
679 long-term aerosol records in the western United States, *J. Geophys. Res.*, **108**, 4623,
680 doi:10.1029/2003JD003459.

681 Yu, H., et al. (2004), The direct radiative effect of aerosols as determined from a
682 combination of MODIS retrievals and GOCART simulations, *J. Geophys. Res.*, **109**,
683 D03206, doi:10.1029/2003JD003914.

684 Yu, H., et al. (2006), A review of measurement-based assessments of the aerosol direct
685 radiative effect and forcing, *Atmos. Chem. Phys.*, **6**, 613-666, doi:10.5194/acp-6-
686 613-2006.

687 Yu, H., L. A. Remer, M. Chin, H. Bian, R. G. Kleidman, and T. Diehl (2008), A satellite-
688 based assessment of transpacific transport of pollution aerosol, *J. Geophys. Res.*,
689 **113**, D14S12, doi:10.1029/2007JD009349.

690 Yu, H., M. Chin, L. A. Remer, R. G. Kleidman, N. Bellouin, H. Bian, and T. Diehl
691 (2009), Variability of marine aerosol fine-mode fraction and estimates of
692 anthropogenic aerosol component over cloud-free oceans from the Moderate
693 resolution Imaging Spectroradiometer (MODIS), *J. Geophys. Res.*, **114**,
694 D10206,10.1029/2008JD010648.

695 Yu, H., L. A. Remer, M. Chin, H. Bian, Q. Tan, T. Yuan, and Y. Zhang (2012a),
696 Aerosols from overseas rival domestic emissions over North America, submitted to
697 *Science*.

698 Yu, H., et al. (2012b), Satellite perspective of aerosol intercontinental transport,
699 submitted to *Atmos. Res.*

700 Zhou, M., H. Yu, R. E. Dickinson, O. Dubovik, and B. N. Holben (2005), A normalized
701 description of the direct effect of key aerosol types on solar radiation as estimated
702 from AERONET aerosols and MODIS albedos. *J. Geophys. Res.*, **110**, D19202,
703 10.1029/2005JD005909.

704

705 **Table Captions**

706

707 **Table 1.** List of 10 models that participated in HTAP aerosol S/R experiments and are
708 used in this analysis.

709

710 **Table 2.** Comparisons of AOD at 550 nm (τ) from 9 HTAP models in this study with that
711 inferred from Schulz et al. (2006). For SO₄ and POM, AOD is inferred by using
712 anthropogenic AOD and anthropogenic fraction of present day AOD. For BC, we infer
713 AOD from the anthropogenic absorptive AOD reported in Schulz et al. [2006] by
714 assuming that all BC is anthropogenic and BC has a single scattering albedo of 0.2 at
715 550 nm.

716

717 **Table 3.** Annual mean aerosol direct radiative forcing normalized by AOD at 550 nm
718 (NDRF, $\text{Wm}^{-2}\tau^{-1}$) at top of atmosphere (TOA) and surface for SO₄, POM, and BC) in
719 the four source regions (NA, EU, EA, SA) and globe, which is derived from
720 GOCART simulated monthly AOD and DRF for 2001.

721

722 **Table 4.** Change of global annual mean AOD ($\tau \times 1000$, mean \pm std. dev) in response to
723 the 20% reduction of anthropogenic emissions in 4 source regions (SR6 - SR1) of 9
724 HTAP models.

725

726 **Table 5.** Change of global annual mean aerosol DRF (unit: mWm^{-2} , mean \pm standard
727 deviation, $1 \text{ mWm}^{-2} = 0.001 \text{ Wm}^{-2}$) in response to the 20% reduction of anthropogenic
728 emissions in 4 source regions as derived from analysis of SR1 and SR6 runs of 9
729 HTAP models.

730

731 **Table 6.** Global annual average TOA all-sky forcing efficiency relative to emissions
732 from the source regions (unit: mWm^{-2} per Tg) as derived from 8 HTAP models. The
733 forcing efficiency for SO₄ and POM is calculated with respect to SO₂ and primary
734 POM emissions, although some models with fully coupled chemistry include changes
735 of SO₄ resulting from the reductions of other emissions and a fraction of POM is
736 secondary aerosol produced from a variety of volatile organic carbon.

737

738 **Table 7:** Response of annual AOD and all-sky DRF (mean \pm std. dev.) in the receptor regions
739 (columns) to 20% reductions of anthropogenic gas and aerosol emissions in the source regions
740 (rows) estimated from 9 HTAP models. Percentage contributions of individual source regions
741 are shown in parentheses for AOD (corresponding percentages for DRF are only slightly
742 different and hence not shown). Contributions of a region on itself (termed “domestic”) are
743 shown in bold. Here BC is listed separately from SO₄ and POM combined (in which SO₄
744 makes a dominant contribution of 69-94%, depending on region), because of their distinct
745 effects on solar radiation. For SO₄+POM, surface DRF is slightly greater than TOA DRF
746 because of weak absorption and not shown. A positive change of DRF for SO₄+POM suggests
747 a weakened cooling effect by the emission reduction. A BC emission reduction introduces a
748 negative change of TOA DRF (a weakened warming effect) and a positive change of surface
749 DRF (a weakened cooling effect).

750

751

752

753 **Figure Captions**

754

755 **Figure 1:** Illustration of four HTAP defined regions for examining the source-receptor
756 relationships for anthropogenic aerosols: North America (NA, 15°-55°N, 60°W-
757 125°W), Europe (EU, 25°-65°N, 10°W-50°E), East Asia (EA, 15°-50°N, 95°-160°E),
758 and South Asia (SA, 5°-35°N, 50°-95°E). Regional and annual anthropogenic
759 emissions of SO₂, primary POM, and BC from 8 HTAP models (excluding
760 HADGEM2 and ECHAM5) are shown in bar charts, with error bar indicating the
761 range of 8 models.

762

763 **Figure 2:** Annual average AOD for the external mixture of sulfate, POM, and BC
764 simulated by baseline runs of 9 HTAP models.

765

766 **Figure 3:** Comparison of HTAP SR1 9-model median AOD for the external mixture of
767 sulfate, POM, and BC (a) with MODIS-derived anthropogenic AOD over ocean as
768 described in Yu et al. [2009] (b) and Bellouin et al. [2008] (c).

769

770 **Figure 4:** Comparisons of zonal variations of seasonal and 20°N-60°N average AOD for
771 sulfate, POM, and BC combined as simulated by HTAP models (black line for median
772 and shaded area for the range of 9 HTAP models) with the MODIS-derived over-
773 ocean anthropogenic AOD (red line for Yu et al., 2009 and blue line for Bellouin et al.,
774 2008).

775

776 **Figure 5:** Seasonal variations of 9-model average TOA DRF (a), and surface DRF (b) in
777 all-sky conditions (Wm⁻²) for the external mixture of sulfate, POM, and BC as derived
778 from the HTAP baseline simulations (SR1).

779

780 **Figure 6:** Global annual mean forcing efficiency (unit: mWm⁻² per Tg) for sulfate (a) and
781 BC (b) with respect to regional (denoted as NA, EU, EA, and SA) emissions as
782 simulated by 8 HTAP models.

783

784 **Figure 7:** Annual average AOD (x100, top panel) and DRF (mWm^{-2}) at the top of
785 atmosphere (TOA) (middle panel) and at the surface (bottom panel) in all-sky
786 conditions resulting from 20% reductions of regional anthropogenic emissions over
787 North America (NA), Europe (EU), East Asia (EA), and South Asia (SA),
788 respectively. A positive value for DRF represents the reduced aerosol direct radiative
789 forcing resulting from the reduction of emissions. Each of the four source regions is
790 overlaid on corresponding SR6xx-SR1 maps where xx represents NA, EU, EA, and
791 SA. Individual aerosol components are assumed to be mixed externally. The results
792 are based on 9 HTAP models.

793

794 **Figure 8:** Seasonal variations of changes in the all-sky DRF (mWm^{-2}) at surface (SR6-
795 SR1) due to 20% reduction of regional anthropogenic emissions derived from 9 HTAP
796 models. Each of the four source regions is overlaid on corresponding SR6xx-SR1
797 maps where xx represents NA, EU, EA, and SA.

798

799 **Figure 9:** Ten-model (including ECHAM5) derived average relative annual
800 intercontinental response (RAIR) for aerosol optical depth (AOD) in four receptor
801 regions, by chemical component. Standard deviations, as indicated by error bars,
802 reflect the model variability in simulating aerosol transport.

803

804 **Figure 10:** same as Figure 9 but for TOA all-sky DRF.

805

806

Table 1. List of 10 models that participated in HTAP aerosol S/R experiments and are used in this analysis				
Model	Model version	Investigator(s)	Resolution (lon. x lat.)	Major Reference(s)
CAM-CHEM	v3311m13	P. Hess	2.5°x1.875°	<i>Pfister et al., 2008</i>
CAM-CHEM	v3514			
ECHAM5 HAMMOZ	v21	I. Bey, G. Forberth	2.813°x2.813°	<i>Pozzoli et al., 2008a and 2008b</i>
GISS PUCCINI	modelEaer	D. Shindell	5°x4°	<i>Koch et al., 2005; Shindell et al., 2006</i>
GMI	v02a	H. Bian	2.5°x2°	<i>Bian et al., 2009</i>
GOCART	v4p2	M. Chin, T. Diehl	2.5°x2°	<i>Chin et al., 2002, 2007, 2009</i>
HADGEM2	A-v01	N. Bellouin	1.875°x1.25°	<i>Bellouin et al., 2011</i>
INCA	v2	M. Schulz	3.75°x2.5°	<i>Schulz, 2007; Hauglustaine et al., 2004; Textor et al., 2006</i>
LLNL IMPACT	T5a	D. Bergmann, C. S. Atherton	2.5°x2°	<i>Rotman et al., 2004.</i>
SPRINTARS	v356	T. Takemura	1.125°x1.125°	<i>Takemura et al., 2005</i>
<i>Acronyms for model names:</i>				
CAM-CHEM: Community Atmospheric Model – Chemistry version (NCAR, USA)				
ECHAM5-HAMMOZ: Max-Planck Institute for Meteorology Hamburg Climate Model - version 5 with Hamburg Aerosol Model and MOZart chemistry sub-Module				
GISS PUCCINI: Goddard Institute for Space Studies, Physical Understanding of Composition-Climate Interactions and Impacts model (NASA GISS, USA)				
GMI: Global Modeling Initiative (NASA GSFC, USA)				
GOCART: Goddard Chemistry Aerosol Radiation and Transport (NASA GSFC, USA)				
HADGEM2: Hadley Centre Global Environment Model version 2 (Met Office, UK)				
INCA: Interaction of Chemistry and Aerosol (laboratoire des Sciences du Climat et de l'Environnement, France)				
LLNL IMPACT: Integrated Massively Parallel Atmospheric Chemical Transport model (Lawrence Livermore National Laboratory, USA)				
SPRINTARS: Spectral Radiation-Transport Model for Aerosol Species (Kyushu University, Japan)				

809

Table 2. Comparisons of AOD at 550 nm (τ) from 9 HTAP models in this study with that inferred from Schulz et al. (2006). For SO_4 and POM, AOD is inferred by using anthropogenic AOD and anthropogenic fraction of present day AOD. For BC, we infer AOD from the anthropogenic absorptive AOD reported in Schulz et al. [2006] by assuming that all BC is anthropogenic and BC has a single scattering albedo of 0.2 at 550 nm.

	This study	Schulz et al. [2006]
τ_{SO_4}	0.0335 ± 0.0134	0.0345 ± 0.0164
τ_{POM}	0.0108 ± 0.0047	0.0151 ± 0.0094
τ_{BC}	0.0022 ± 0.0010	0.0024 ± 0.0010

810

811

812

Table 3. Annual mean aerosol direct radiative forcing normalized by AOD at 550 nm (NDRF, $\text{Wm}^{-2}\tau^{-1}$) at top of atmosphere (TOA) and surface for SO_4 , POM, and BC) in the four source regions (NA, EU, EA, SA) and globe, which is derived from GOCART simulated monthly AOD and DRF for 2001.

Sky Condition	Region	NDRF _{SO4}		NDRF _{POM}		NDRF _{BC}	
		TOA	Surface	TOA	Surface	TOA	surface
All Sky	NA	-24.9	-24.5	-28.4	-39.1	84.6	-225.2
	EU	-21.1	-20.4	-22.6	-32.8	93.0	-190.8
	EA	-21.4	-21.2	-25.4	-35.1	83.2	-210.0
	SA	-24.9	-25.1	-28.7	-41.0	89.6	-235.2
	globe	-24.2	-24.1	-30.0	-41.5	85.9	-231.6
Clear Sky	NA	-30.6	-30.1	-35.4	-45.9	62.1	-246.1
	EU	-25.6	-24.6	-27.9	-37.9	80.2	-207.8
	EA	-26.6	-26.3	-32.1	-41.5	59.9	-231.3
	SA	-27.7	-27.8	-32.7	-44.8	74.6	-247.6
	globe	-30.2	-29.9	-37.0	-48.4	62.8	-252.7

813

814

815

816

Table 4. Change of global annual mean AOD ($\tau \times 1000$, mean \pm std. dev) in response to the 20% reduction of anthropogenic emissions in 4 source regions (SR6 - SR1) of 9 HTAP models.				
Source Region	τ_{SO_4}	τ_{POM}	τ_{BC}	$\tau_{\text{SO}_4+\text{POM}+\text{BC}}$
NA	-0.67 ± 0.23	-0.054 ± 0.036	-0.026 ± 0.013	-0.75 ± 0.23
EU	-1.13 ± 0.47	-0.084 ± 0.058	-0.050 ± 0.021	-1.28 ± 0.45
EA	-0.97 ± 0.38	-0.142 ± 0.101	-0.086 ± 0.047	-1.19 ± 0.37
SA	-0.32 ± 0.11	-0.102 ± 0.059	-0.038 ± 0.019	-0.46 ± 0.10
Total	-3.10 ± 1.11	-0.383 ± 0.246	-0.199 ± 0.093	-3.70 ± 1.08

817

818

Table 5. Change of global annual mean aerosol DRF (unit: mWm^{-2} , mean \pm standard deviation, $1 \text{ mWm}^{-2} = 0.001 \text{ Wm}^{-2}$) in response to the 20% reduction of anthropogenic emissions in 4 source regions as derived from analysis of SR1 and SR6 runs of 9 HTAP models.

Source Region	DRF_{SO_4}	DRF_{POM}	DRF_{BC}	$\text{DRF}_{\text{SO}_4+\text{POM}+\text{BC}}$
All-sky TOA DRF (mWm^{-2})				
NA	15.4 ± 5.1	1.4 ± 0.9	-3.0 ± 1.6	13.8 ± 5.3
EU	24.4 ± 8.9	1.6 ± 1.2	-5.9 ± 2.6	20.2 ± 9.5
EA	19.4 ± 7.9	3.1 ± 2.2	-9.4 ± 6.1	13.0 ± 9.9
SA	6.8 ± 1.9	2.5 ± 1.7	-3.6 ± 1.8	5.7 ± 2.6
Total	66.1 ± 22.8	8.6 ± 5.7	-21.9 ± 11.5	52.8 ± 25.3
All-sky surface DRF (mWm^{-2})				
NA	14.9 ± 4.9	1.9 ± 1.3	5.5 ± 2.4	22.4 ± 5.5
EU	23.0 ± 8.0	2.4 ± 1.7	8.8 ± 3.1	34.1 ± 7.3
EA	18.9 ± 7.5	4.4 ± 3.2	16.5 ± 8.7	39.9 ± 11.7
SA	6.9 ± 2.0	3.6 ± 2.3	8.1 ± 3.6	18.6 ± 4.6
Total	63.7 ± 21.4	12.3 ± 8.1	39.0 ± 16.6	115.0 ± 26.0

820

821

822

823

Table 6. Global annual average TOA all-sky forcing efficiency relative to emissions from the source regions (unit: mWm^{-2} per Tg) as derived from 8 HTAP models. The forcing efficiency for SO_4 and POM is calculated with respect to SO_2 and primary POM emissions, although some models with fully coupled chemistry include changes of SO_4 resulting from the reductions of other emissions and a fraction of POM is secondary aerosol produced from a variety of volatile organic carbon.

Source Region	SO_4	POM	BC
NA	-3.6 ± 1.0	-4.3 ± 1.5	27.2 ± 14.2
EU	-3.7 ± 1.1	-4.2 ± 1.6	36.7 ± 18.0
EA	-2.7 ± 0.9	-3.6 ± 1.7	27.7 ± 19.0
SA	-3.8 ± 1.0	-4.0 ± 1.7	25.0 ± 13.6
Total	-3.3 ± 0.9	-3.9 ± 1.6	29.0 ± 16.8

824

825

Table 7: Response of annual AOD and all-sky DRF (mean \pm std. dev.) in the receptor regions (columns) to 20% reductions of anthropogenic gas and aerosol emissions in the source regions (rows) estimated from 9 HTAP models. Percentage contributions of individual source regions are shown in parentheses for AOD (corresponding percentages for DRF are only slightly different and hence not shown). Contributions of a region on itself (termed “domestic”) are shown in bold. Here BC is listed separately from SO₄ and POM combined (in which SO₄ makes a dominant contribution of 69-94%, depending on region), because of their distinct effects on solar radiation. For SO₄+POM, surface DRF is slightly greater than TOA DRF because of weak absorption and not shown. A positive change of DRF for SO₄+POM suggests a weakened cooling effect by the emission reduction. A BC emission reduction introduces a negative change of TOA DRF (a weakened warming effect) and a positive change of surface DRF (a weakened cooling effect).

	Receptor Region			
Source Region	NA	EU	EA	SA
SO ₄ +POM AOD (x1000)				
NA	-8.53±2.85 (82%)	-1.22±0.66 (7%)	-0.35±0.25 (2%)	-0.24±0.22 (2%)
EU	-0.42±0.21 (4%)	-13.81±4.43 (84%)	-1.21±0.68 (6%)	-2.18±0.79 (16%)
EA	-0.92±0.59 (9%)	-0.65±0.48 (4%)	-16.42±5.02 (84%)	-1.05±0.66 (8%)
SA	-0.54±0.91 (5%)	-0.72±1.32 (4%)	-1.68±0.95 (9%)	-10.37±3.21 (75%)
BC AOD (x1000)				
NA	-0.28±0.09 (65%)	-0.05±0.04 (8%)	-0.02±0.01 (1%)	-0.01±0.01 (1%)
EU	-0.02±0.02 (4%)	-0.51±0.15 (76%)	-0.05±0.03 (4%)	-0.08±0.04 (8%)
EA	-0.10±0.09 (23%)	-0.07±0.08 (10%)	-1.04±0.28 (84%)	-0.09±0.06 (9%)
SA	-0.04±0.03 (8%)	-0.04±0.03 (6%)	-0.14±0.08 (11%)	-0.87±0.36 (82%)
SO ₄ +POM all-sky TOA DRF (mWm ⁻²)				
NA	207.7±68.9	28.8±14.9	7.5±5.2	6.3±5.7
EU	10.4±5.42	304.4±93.3	25.4±14.1	54.2±20.3
EA	23.8±15.1	14.4±10.9	315.2±98.8	25.0±15.5
SA	11.2± 15.5	8.8±9.4	32.9±15.4	256.4±80.4
BC all-sky TOA DRF (mWm ⁻²)				
NA	-23.8±7.2	-5.1±3.3	-1.4±1.3	-1.5±1.3
EU	-1.7±1.4	-45.6±12.8	-4.5±2.7	-9.2±4.4
EA	-9.0±8.5	-6.7±7.3	-83.5±22.3	-8.6±6.5
SA	-3.0±2.3	-4.1±2.7	-11.8±5.3	-70.7±29.6
BC all-sky surface DRF (mWm ⁻²)				
NA	64.1±20.5	11.5±7.2	3.3±3.0	3.5±2.8
EU	4.3±3.5	103.0±27.1	10.0±5.9	19.8±9.9
EA	22.7±21.6	14.4±15.5	212.8±57.0	22.3±15.0
SA	7.9±6.2	7.5±5.3	29.3±13.5	202.0±85.4

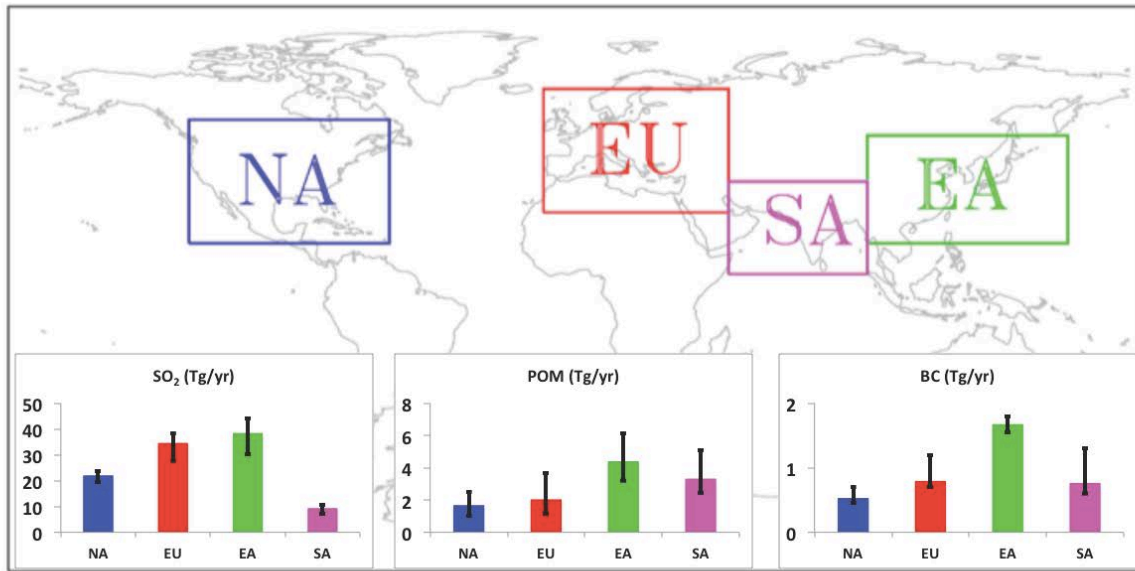


Figure 1: Illustration of four HTAP defined regions for examining the source-receptor relationships for anthropogenic aerosols: North America (NA, 15°-55°N, 60°W-125°W), Europe (EU, 25°-65°N, 10°W-50°E), East Asia (EA, 15°-50°N, 95°-160°E), and South Asia (SA, 5°-35°N, 50°-95°E). Regional and annual anthropogenic emissions of SO₂, primary POM, and BC from 8 models (excluding HADGEM2 and ECHAM5) are shown in bar charts, with error bar indicating the range of 8 models.

829

830

831

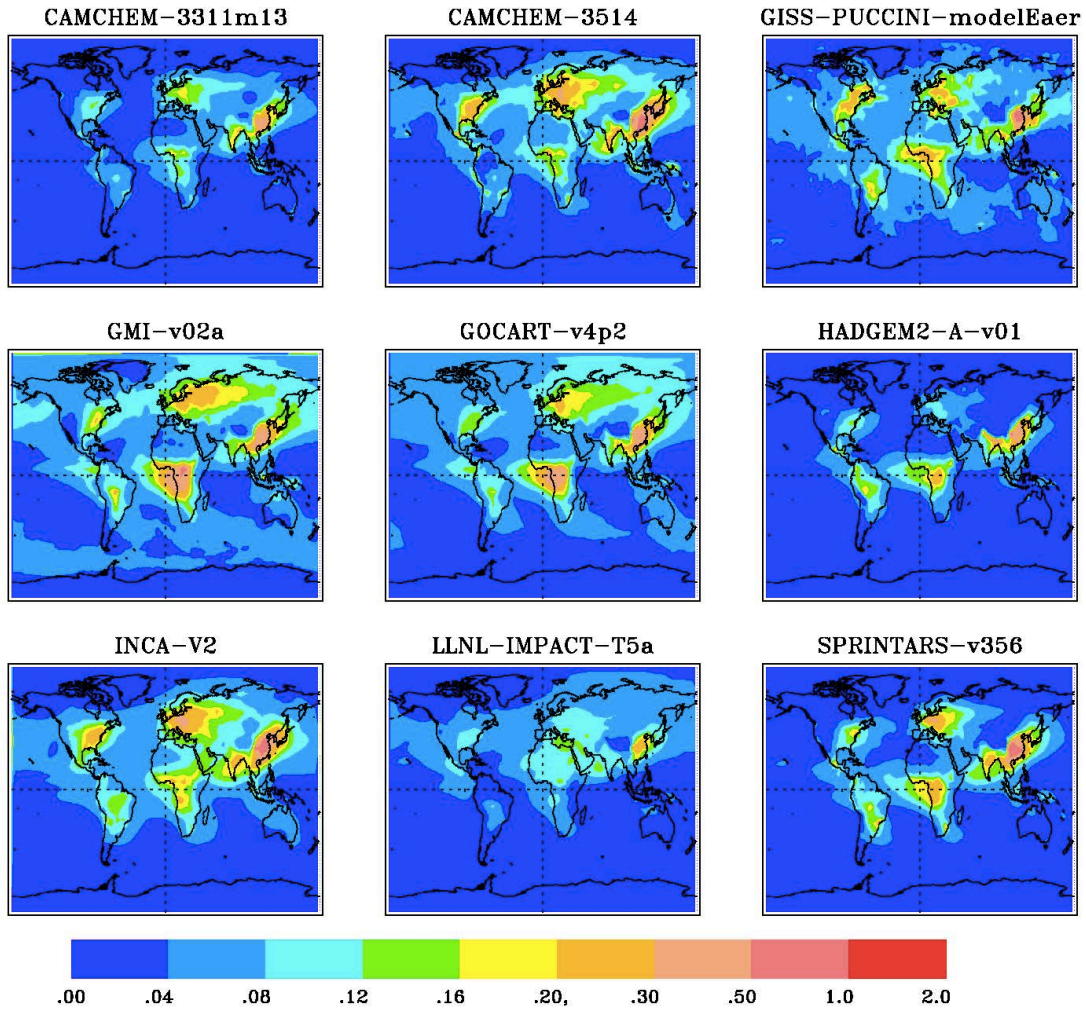
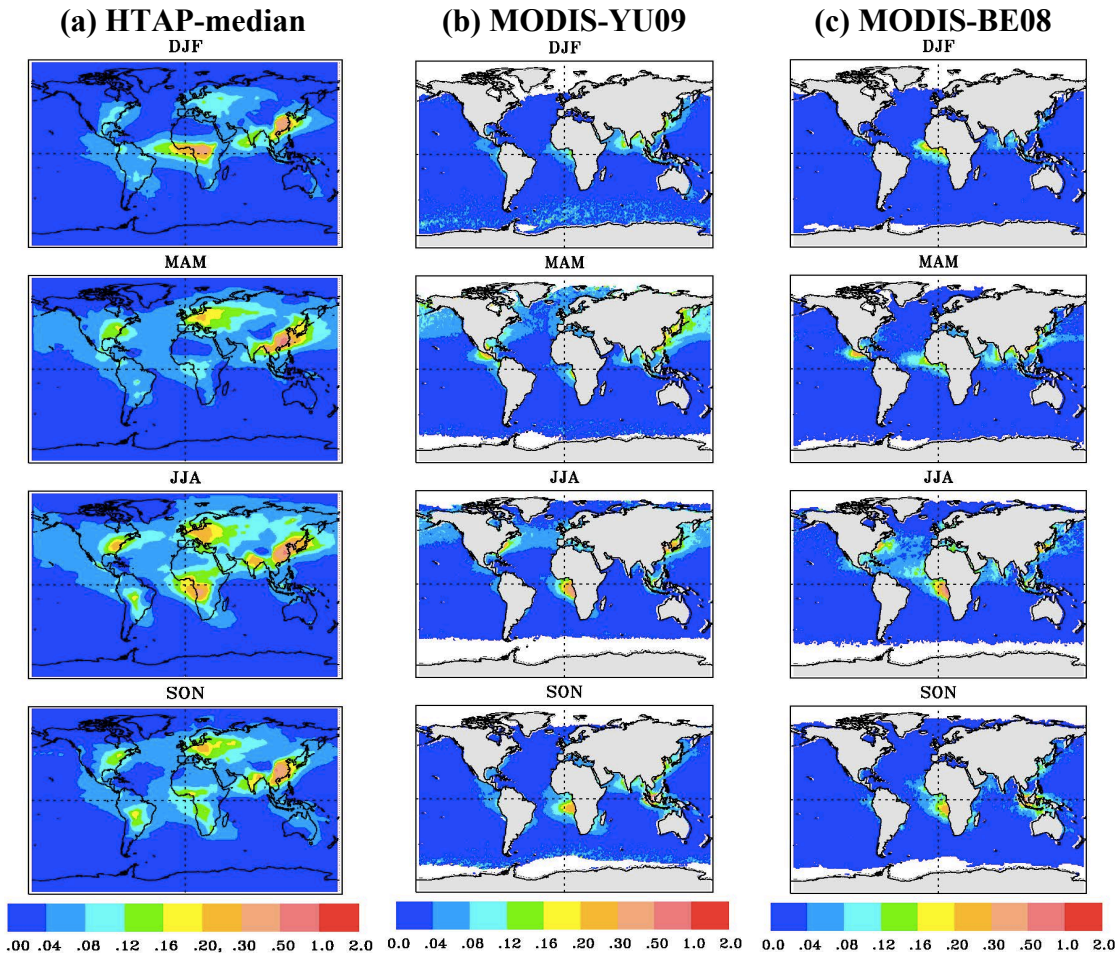


Figure 2: Annual average AOD for the external mixture of sulfate, POM, and BC simulated by baseline runs of 9 HTAP models.

835



836

837

838

839

840

841

842

843

Figure 3: Comparison of HTAP SR1 9-model median AOD for the external mixture of sulfate, POM, and BC (a) with MODIS-derived anthropogenic AOD over ocean as described in Yu et al. [2009] (b) and Bellouin et al. [2008] (c).

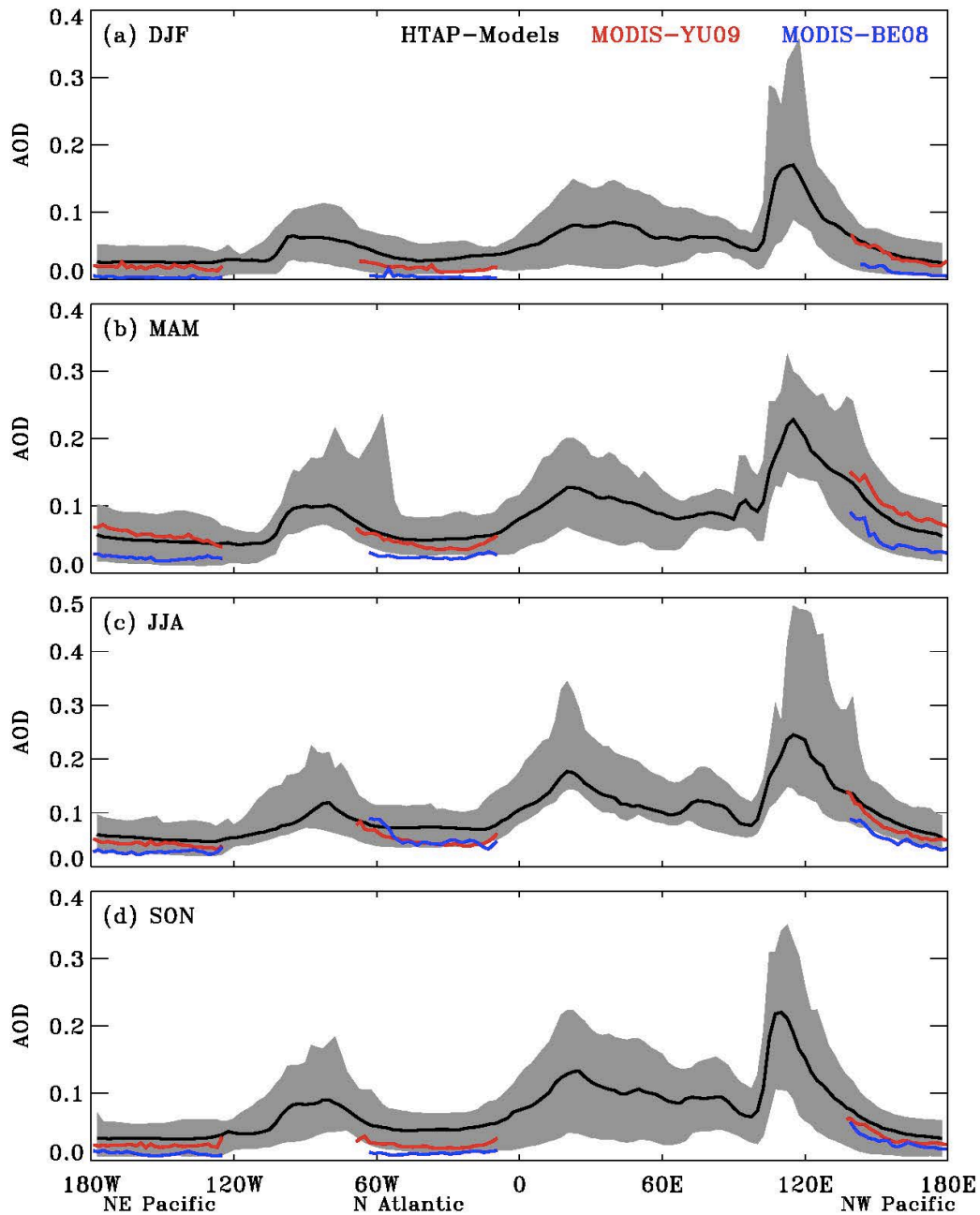


Figure 4: Comparisons of zonal variations of seasonal and 20°N - 60°N average AOD for sulfate, POM, and BC combined as simulated by HTAP models (black line for median and shaded area for the range of 9 models) with the MODIS-derived over-ocean anthropogenic AOD (red line for *Yu et al., 2009* and blue line for *Bellouin et al., 2008*). Note that HTAP model results cover both land and ocean, while MODIS-based anthropogenic AOD were estimated only over ocean.

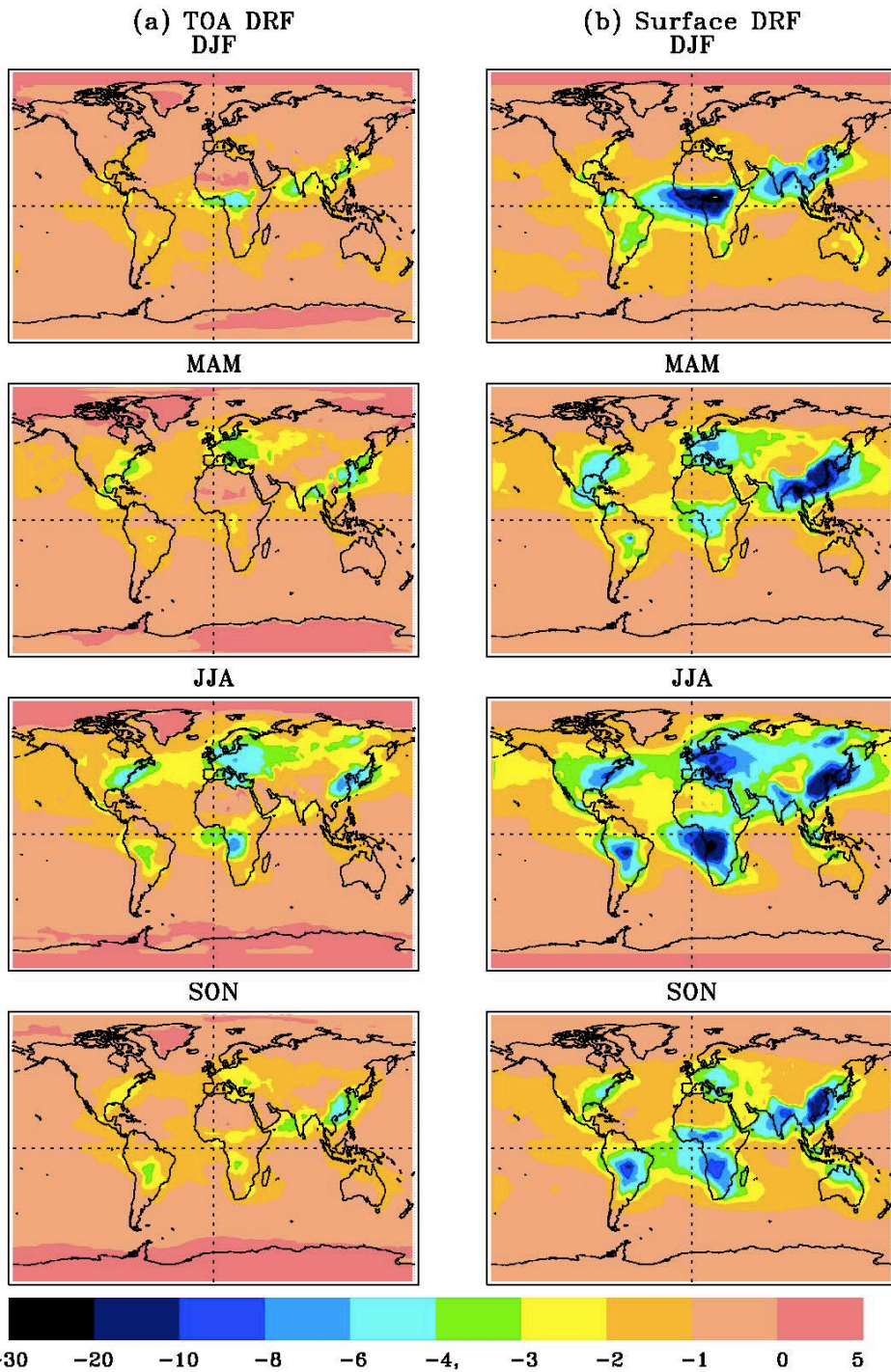


Figure 5: Seasonal variations of 9-model average TOA DRF (a), and surface DRF (b) in all-sky conditions (Wm^{-2}) for the external mixture of sulfate, POM, and BC as derived from the HTAP baseline simulations (SR1).

848
849

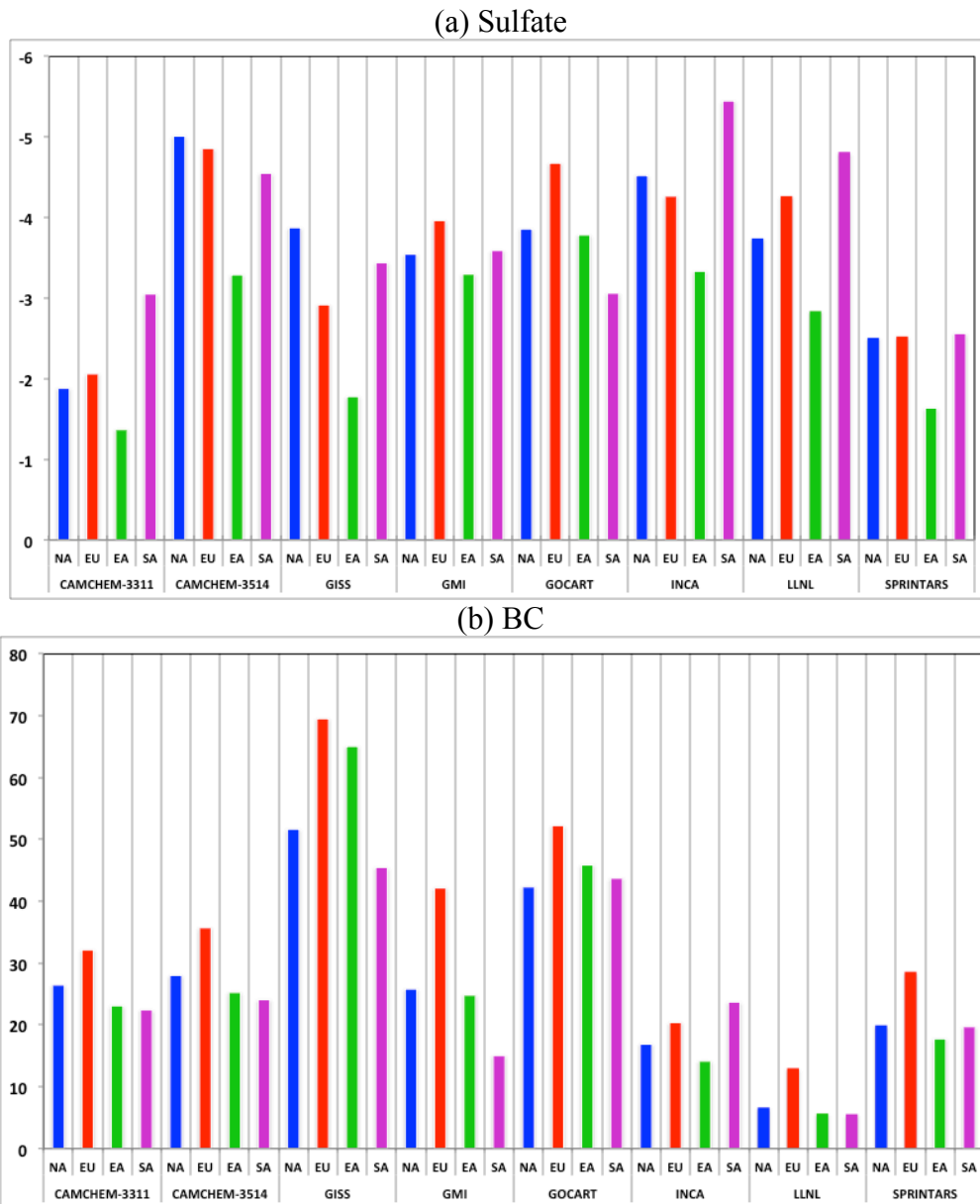


Figure 6: Global annual mean forcing efficiency (unit: mWm^{-2} per Tg) for sulfate (a) and BC (b) with respect to regional (denoted as NA, EU, EA, and SA) emissions as simulated by 8 HTAP models.

850
851

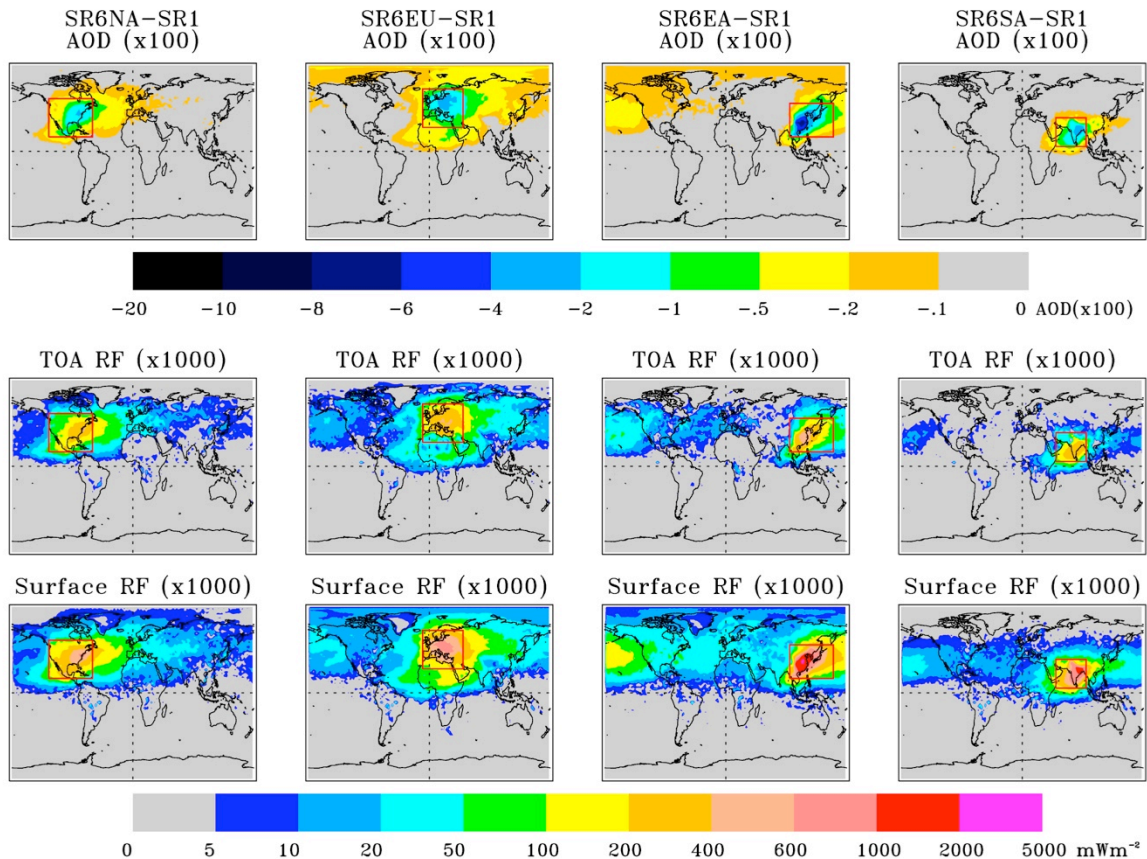


Figure 7: Annual average AOD (x100, top panel) and DRF (mWm^{-2}) at the top of atmosphere (TOA) (middle panel) and at the surface (bottom panel) in all-sky conditions resulting from 20% reductions of regional anthropogenic emissions over North America (NA), Europe (EU), East Asia (EA), and South Asia (SA), respectively. A positive value for DRF represents the reduced aerosol direct radiative forcing resulting from the reduction of emissions. Each of the four source regions is overlaid on corresponding SR6xx-SR1 maps where xx represents NA, EU, EA, and SA. Individual aerosol components are assumed to be mixed externally. The results are based on 9 HTAP models.

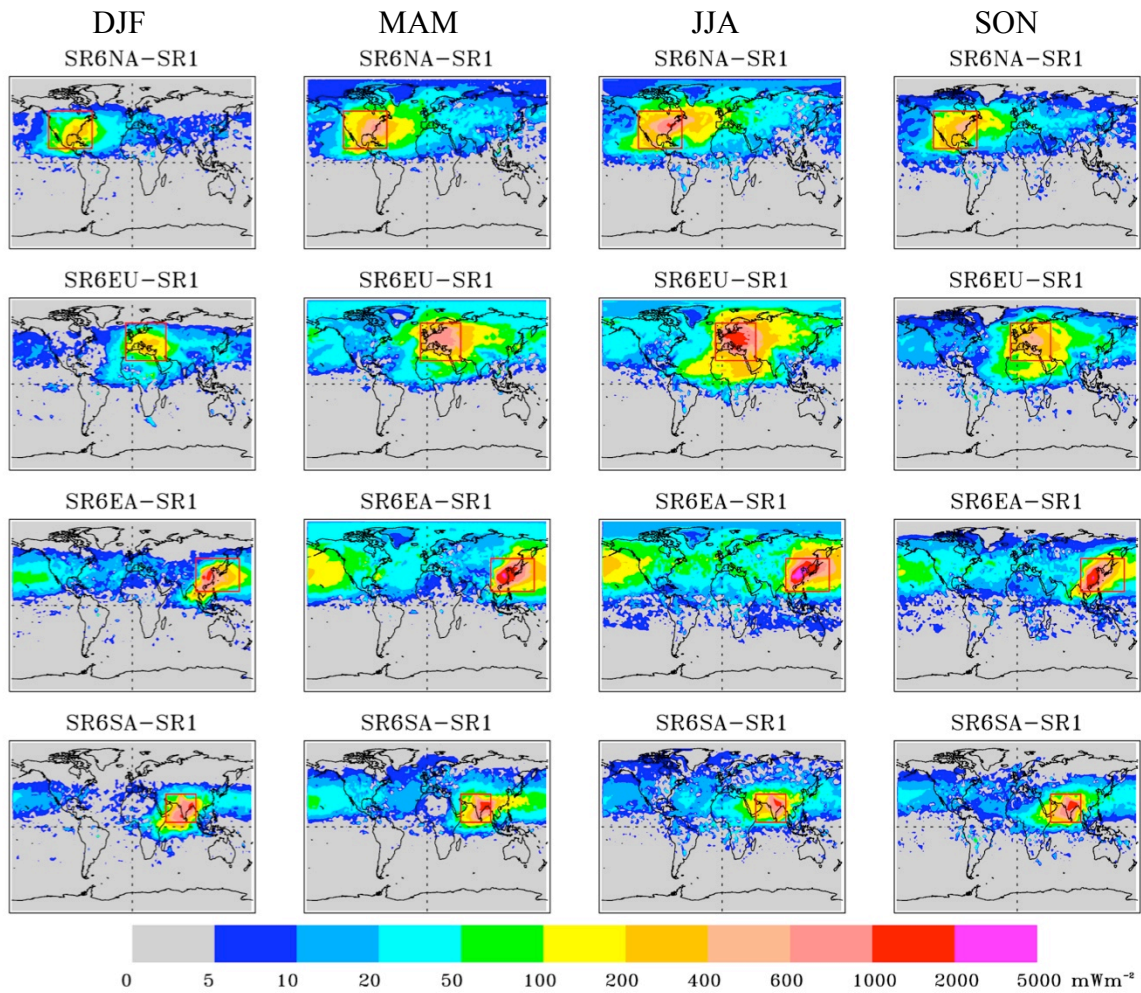


Figure 8: Seasonal variations of changes in the all-sky DRF (mWm^{-2}) at surface (SR6-SR1) due to 20% reduction of regional anthropogenic emissions derived from 9 HTAP models. Each of the four source regions is overlaid on corresponding SR6xx-SR1 maps where xx represents NA, EU, EA, and SA.

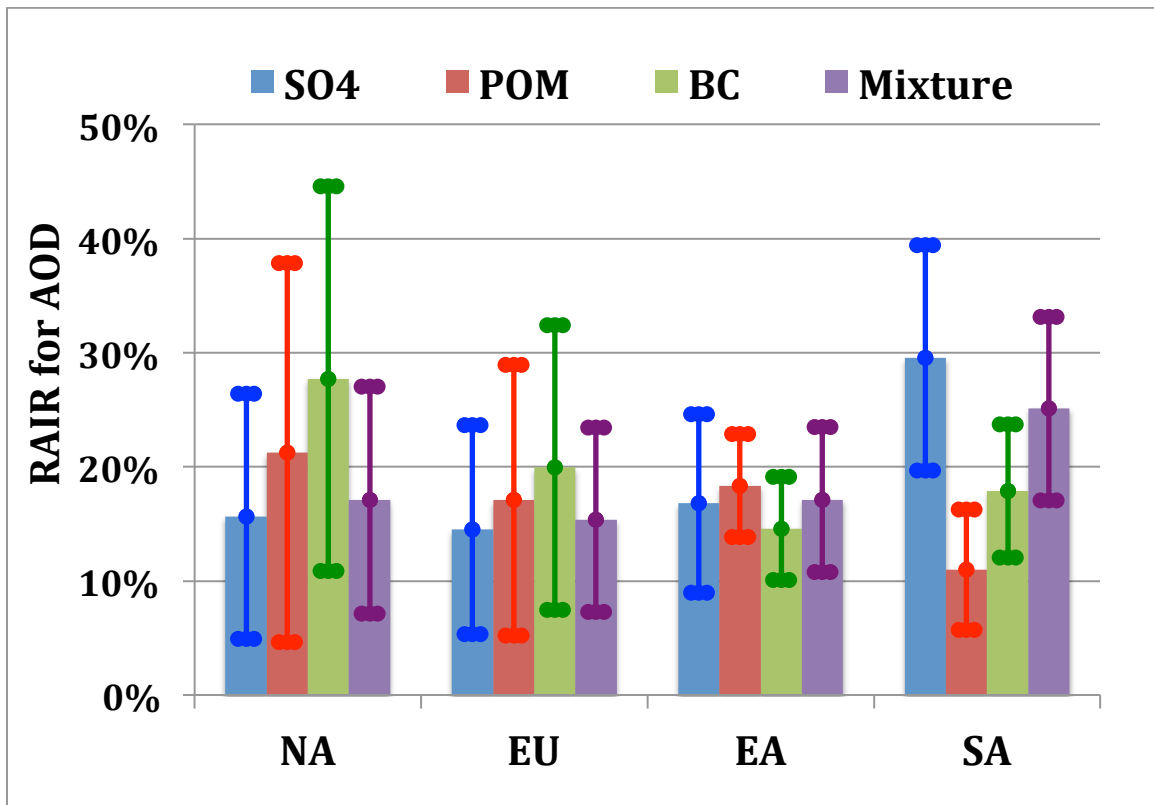


Figure 9: Ten-model (including ECHAM5) derived average relative annual intercontinental response (RAIR) for aerosol optical depth (AOD) in four receptor regions, by chemical component. Standard deviations, as indicated by error bars, reflect the model variability in simulating aerosol transport.

856
857
858

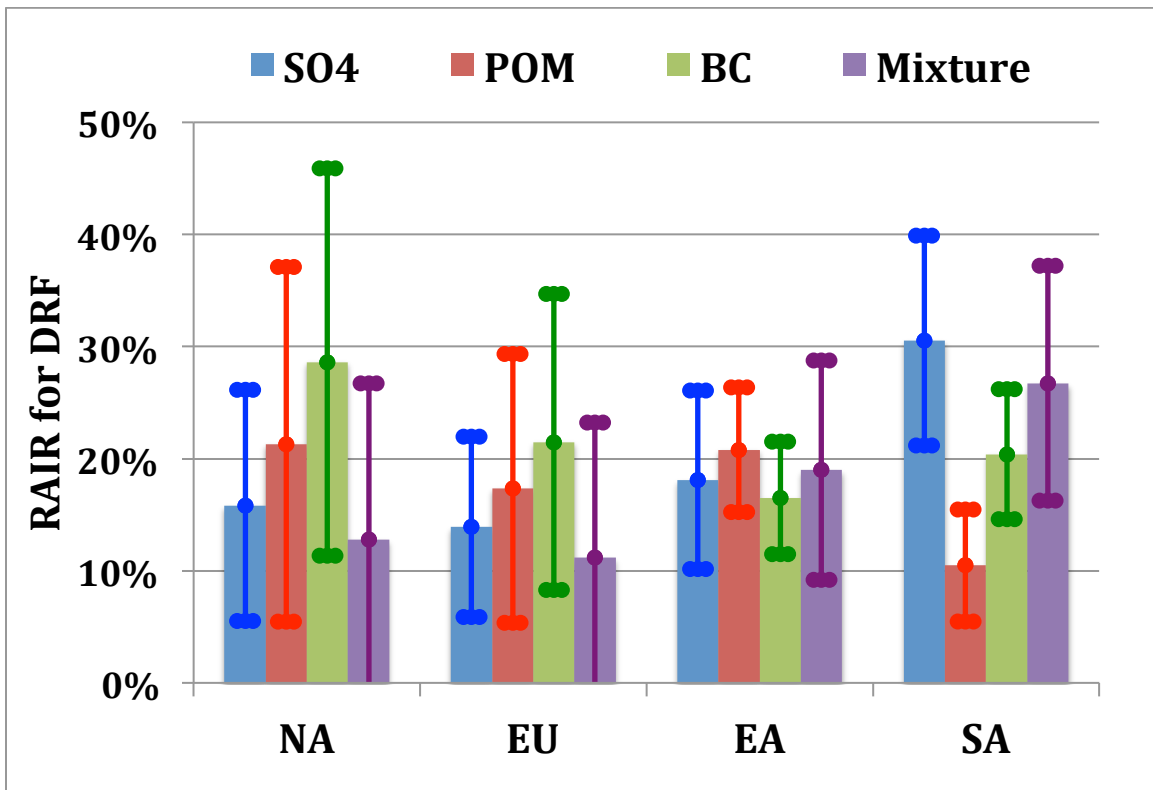


Figure 10: same as Figure 9 but for TOA all-sky DRF.